

Article

Feed Drive Control and Non-Linear Friction Interaction Effect on Machining Chatter Stability Prediction

Oier Franco ^{1,*} , Xavier Beudaert ¹, Kaan Erkorkmaz ² and Jokin Munoa ^{1,3} 

¹ Dynamics and Control, Ideko, 20870 Elgoibar, Spain; xbeudaert@ideko.es (X.B.); jmunoa@ideko.es (J.M.)

² Precision Controls Laboratory, University of Waterloo, Waterloo, ON N2L 3G1, Canada; kaane@uwaterloo.ca

³ Department of Mechanical Engineering, University of the Basque Country, 48013 Bilbao, Spain

* Correspondence: ofranco@ideko.es

Abstract: In large-scale machine tool applications, the presence of low structural natural frequencies limits the cutting capabilities of the machine. The machine tool joints interact with the structural mode shapes, hence, the feed drive system characteristics can significantly influence the resultant dynamics at the cutting point. This paper investigates the effect of guideway non-linear friction and feed drive motion control parameters on chatter stability predictions. Field experimentation on seven machines reveals substantial differences between in-motion and idle dynamics, leading to errors in traditional process stability predictions. By using a one-degree-of-freedom model that incorporates non-linear friction and controller forces together with motion commands, the effect of axis motion on machine tool dynamics is analyzed. Later, the feed and force non-linearities are studied in a large-scale machine tool using traditional and alternative dynamic characterization techniques. The findings demonstrate that both feed and force non-linearities influence the frequency response functions at the cutting points, ultimately affecting the accuracy of process stability predictions. Proper selection of feed drive control parameters reduces the cutting point compliance, improving machine tool productivity by up to 50%.

Keywords: machine tool dynamics; feed drives; friction; chatter; control



Citation: Franco, O.; Beudaert, X.; Erkorkmaz, K.; Munoa, J. Feed Drive Control and Non-Linear Friction Interaction Effect on Machining Chatter Stability Prediction. *J. Manuf. Mater. Process.* **2024**, *8*, 207. <https://doi.org/10.3390/jmmp8050207>

Academic Editors: Zekai Murat Kilic, Jixiang Yang and Mohit Law

Received: 5 July 2024

Revised: 16 September 2024

Accepted: 20 September 2024

Published: 24 September 2024



Copyright: © 2024 by the authors. Licensee MDPI, Basel, Switzerland. This article is an open access article distributed under the terms and conditions of the Creative Commons Attribution (CC BY) license (<https://creativecommons.org/licenses/by/4.0/>).

1. Introduction

The occurrence of self-excited vibration during the cutting process remains a significant obstacle to increasing machine tool productivity (Munoa et al. [1]). To predict and prevent this undesired phenomenon, the computation of stability lobe diagrams is widely used. However, uncertainties arise, particularly concerning the dynamic characteristics of the machining system and material cutting coefficients, as initially concluded by Brecher and Esser [2]. Subsequent studies, such as that by Rasper et al. [3], have identified the reliable characterization of machine tool compliance as a key factor influencing chatter stability predictions. To accurately characterize the machining system dynamics under real manufacturing conditions, various alternative experimental methods for machine tool dynamics identification have been proposed, as summarized by Iglesias et al. [4].

In large-scale machine tool applications, productivity limitations often stem from critical resonances associated with structural modal shapes, which involve different components of the machine, such as ram, saddle, column, etc. Such modal shapes frequently imply relative motion between these elements through the axes joints, where the feed drive control system encoders and axes guideways are present. The effect of the feed drive control commissioning and existing friction on the guideway system on the machine tool dynamics have been previously studied in the literature.

On one hand, low-frequency structural resonances involving relative motion among machine tool components can be observed through the feed drive control feedback system, making its parametrization a non-trivial task. While variations of industrially established

control schemes exist in the literature to enhance the control system bandwidth (Xu et al. 2023 [5], Sun et al. 2018 [6], Neubauer et al. [7] or Zhang [8]) or to actively damp chatter vibrations (Dumanli et al. [9,10] or Kakinuma et al. [11]), the standard control configuration can also contribute to increase the damping of the mechanical system (Uriarte et al. [12], Altintas et al. [13]). The prevailing trend in the industry is to maximize the achievable velocity and position loop bandwidth to enhance the machine tool tracking performance. However, this approach can limit the damping provided by the feed drive control system, potentially compromising the dynamic behavior at the cutting point. In the past, different researchers investigated the influence of the motion control parameters on the machine tool dynamic behavior. In 2008, Zirn [14] found that among the main control gains in standard feed drive control, the velocity proportional gain has the most significant impact on the damping added by the feed drive system. This finding was experimentally validated by Franco et al. [15] on a large-scale vertical lathe driven by a double pinion and rack mechanism. Grau et al. [16] also analyzed the effect of the position proportional loop gain on a vertical machining center. Albertelli et al. [17] simulated the effect of feed drive control parametrization on chatter stability limits, concluding that proper control tuning could affect the machining capabilities. In 2020, Beudaert et al. [18] proposed a control tuning strategy that increased the experimental cutting capabilities by up to 30% in a linear motor-driven milling machine.

On the other hand, guideway friction stands out as the primary source of disturbances in the machine tool industry, often causing positioning errors during motion, especially during velocity reversals [19]. The imperative to construct faster and more precise machines has prompted significant advancements in reducing friction in components experiencing relative motions. In 1970, Koenigsberger and Tlustý [20], along with Zhang et al. [21] in 2003, determined that a significant portion of machine tool damping originates from the machine tool joints. Consequently, the damping contributed by the machine guiding system emerges as a crucial parameter in determining machine tool dynamics and, consequently, the process stability. Friction has been extensively examined to ensure accurate motion positioning, as summarized by Armstrong et al. [22] in 1994, and recent studies have investigated the influence of friction on the structural response. In 2014, Bianchi et al. [23] developed a simulation model to analyze the dynamic response of the tool center point under the influence of friction and servo dynamics, albeit without experimental validation. Subsequently, in 2019, Zaeh et al. [24] proposed a machine tool model that accounts for linear and non-linear damping sources, such as friction. They demonstrated that beyond a critical feedrate, the damping ratio of a specific vibration mode remains relatively constant. Similarly, Sato et al. [25] compared the compliance of a machine tool axis under idle and moving conditions, while Oshita et al. [26] illustrated variations in both the stiffness and damping properties of a linear guide for different sliding velocities in the traverse direction. In 2021, Tunc et al. [27] reported significant differences in the measured tool center point compliance of a milling-capable robot between idle and in-motion states, emphasizing the need for further modeling to understand the underlying causes. Building upon this, in 2022, Franco et al. [28] demonstrated that existing guideway non-linear friction can profoundly influence the structural dynamics of a machine tool, resulting in substantial disparities in receptance measurements between idle and in-motion conditions.

Machine tool dynamics are often characterized in idle conditions through impact hammer testing, which may not fully capture the influence of the feed drive control parameters on the tool center point compliance. In cutting applications such as milling, where the axis traverse velocity can be high enough to place the axis in the viscous dominated portion of the friction characteristics, significant dynamic behavior variations can be faced between idle and operating conditions, which will also impact the prediction accuracy of the computed stability lobe diagrams.

Therefore, this paper presents an examination of the influential role of friction on predicted stability lobes, highlighting its impact on both the dynamic response of the machine and subsequent stability predictions. Consequently, based on the concept of 'invariant FRF',

this paper guides the tuning of the feed drive controller to maximize the cutting capabilities of the driven machine. By integrating modeling techniques and experimental testing, the combined effect of feed drive non-linear friction and controller parametrization is validated in a single-degree-of-freedom test bench and in an industrial large-scale machine tool. Additionally, this paper offers a comparative analysis of stability predictions based on classical and alternative dynamic characterizations techniques, providing valuable insight into optimizing control strategies for enhanced machining performance.

This paper is organized as follows: Section 2 presents experimental findings gathered from seven different industrial machine tools, revealing significant and frequently occurring dynamic variations between in-motion and idle states. Next, Section 3 describes the different dynamic characterization techniques used in this research. Section 4 introduces a one-degree-of-freedom time-domain simulation model, which comprehensively incorporates the influence of non-linear friction, structural dynamics, a feed drive control system and machine movements. Then, the experimental validation of both a laboratory single-axis test bench and an industrial large-scale moving column machine are presented in Sections 5 and 6, respectively, showcasing the prediction error of the chatter stability boundary prediction.

2. Comparative Analysis of Idle and In-Motion Experimental Dynamic Responses

The influence of the axis velocity on the cutting point compliance has been assessed across seven distinct machine tools, comprising two large portal milling machines, three ram-type milling machines, one turning machine and a robot equipped with a milling spindle (see Figure 1). In all the experimental characterizations, each cartesian axis (xyz) is commanded with a back-and-forth movement at the same axis velocity, resulting in a three-axis linear interpolation trajectory of the tool center point. The axis displacements are lower than 40 mm to ensure that the observed dynamic compliance variations are not influenced by posture changes. All the measurements presented in this section were obtained from impact hammer tests (maximal impact force of 2000 N) performed after the axis inversion to avoid motion reversals and transient effects. The measurements do not show a significant influence of the axis traveling direction on the tool tip dynamics; hence, this effect is discarded here. Magnitude values are not disclosed due to confidentiality, and alternative values labeled ‘a’ are used to protect sensitive data.

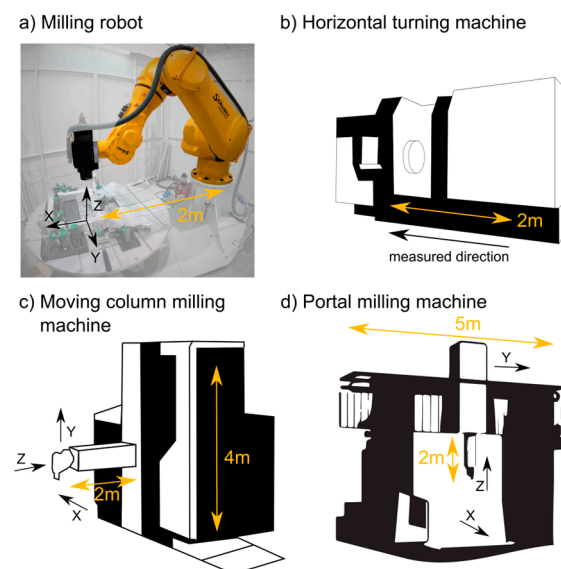


Figure 1. Graphical summary of the tested machine configurations.

2.1. Milling Robot

The first machine under analysis is an industrial robot equipped with a milling spindle head (STAUBLI TX200), as depicted in Figure 2, illustrating the nine direct and cross-compliances across the three cartesian directions. Initially, with each joint of the robot braked, the system exhibits a highly undamped response. However, upon energizing the joints and activating each joint controller, the initial damping values for the resonance increase. A 10 mm/min trajectory in cartesian direction is commanded in *xyz*-directions (meaning that six robot joints have variable speed). As the joints begin to move, the response becomes further damped, particularly noticeable in the Φ_{zz} direct response. Here, the response diminishes by 50% upon removing the axis brakes and by 77% upon initiating axis movement. Future investigations are needed to analyze these non-cartesian structures in assessing the impact of each articulation on the overall system.

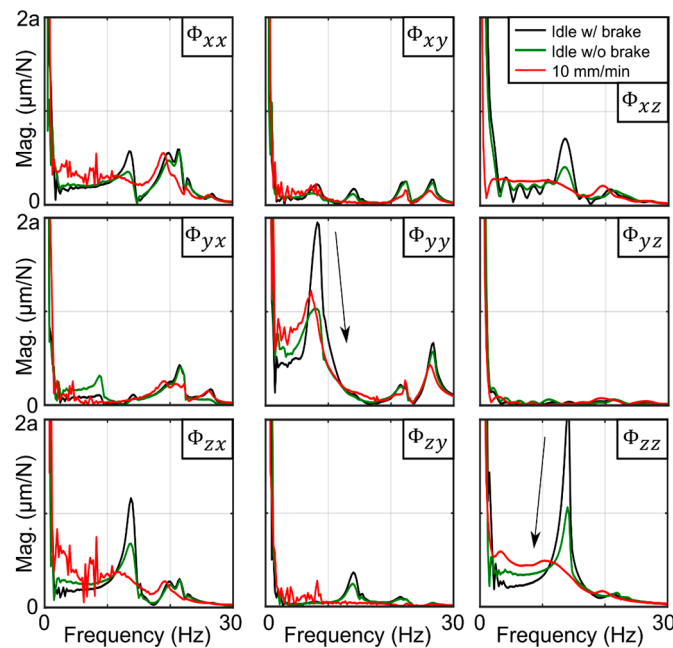


Figure 2. Idle and moving FRF for a robot with milling capabilities.

2.2. Horizontal Turning Machine Turret

Figure 3 shows the direct compliance of the longitudinal axes of a horizontal lathe (see Figure 1b for clarification on moving direction) driven by a ball screw drive and that uses friction guides with Turcite®. The frequency response function is notably influenced by motion, particularly evident in the primary resonance around 95 Hz and in the low-frequency range (<50 Hz). Additionally, the measured response exhibits a high level of fidelity and consistency (coherence > 0.9), indicating good quality of the obtained data.

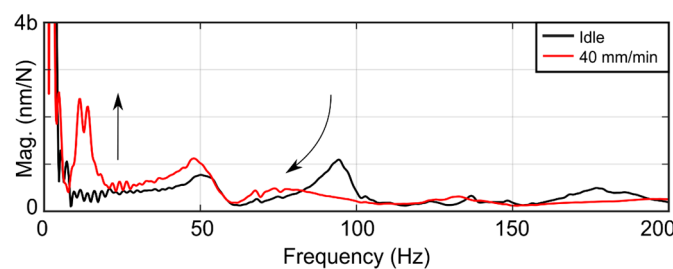


Figure 3. Idle and moving FRF for a horizontal lathe.

2.3. Moving Column Milling Machine

Three different moving column machine tools have been dynamically characterized (Figure 1c). In these machines, the horizontal x -axis is driven by a double pinion and rack feed drive system, while the vertical and ram axes (y and z , respectively) utilize ball screw feed drives. Notably, the vertical axis incorporates a hydro-pneumatic accumulator for weight compensation. Due to the considerable ram overhang, the x - and y -directions are typically the most flexible, with dynamic responses often governed by ram bending resonances. Figure 4a illustrates the nine direct and cross-FRFs under both idle and moving conditions, revealing significant modifications in the vertical direct compliance (Φ_{yy}). This frequency alteration also impacts cross-compliances, such as Φ_{xy} and Φ_{yx} , with the primary resonance experiencing increased damping. In Figure 4b, a second moving ram traveling-type machine exhibits a similar trend to the previous one. Here, notable compliance variations are observed in the direct vertical FRF (Φ_{yy}). Additionally, the feed influence leads to a significant increase in damping in cross-FRFs, such as Φ_{xy} , Φ_{yx} , Φ_{yz} and Φ_{zy} .

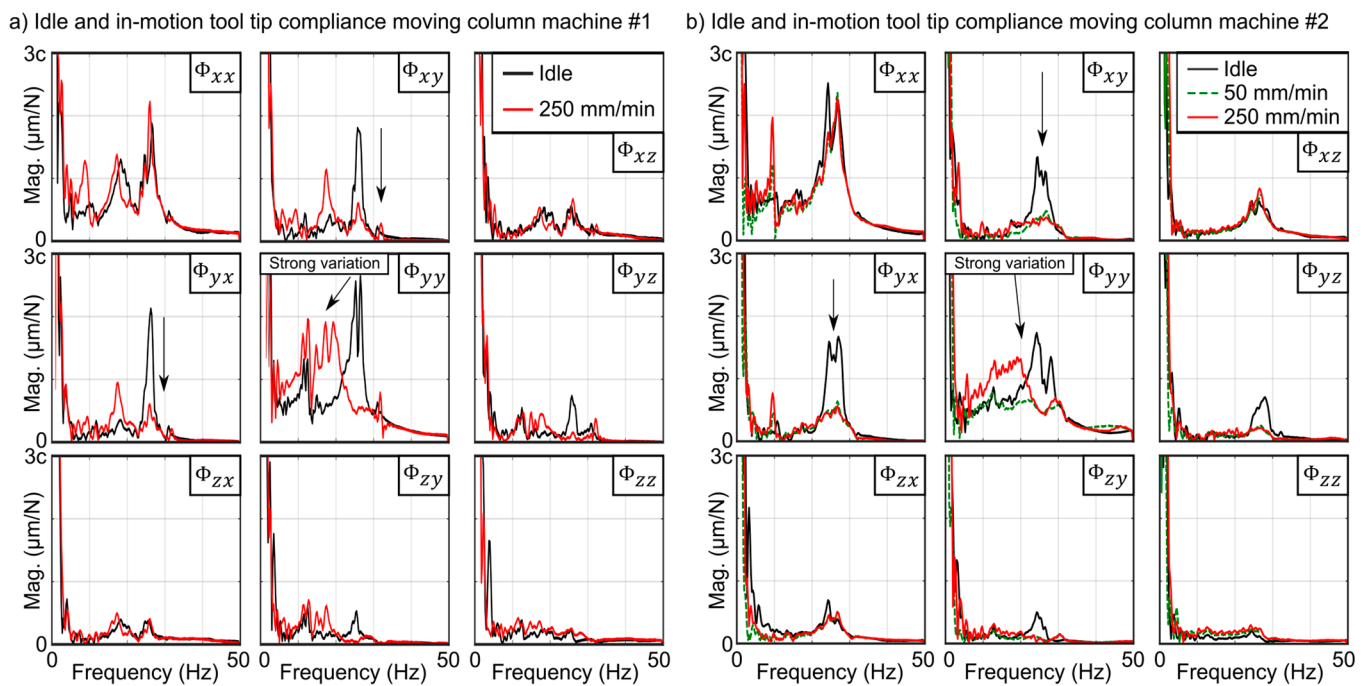


Figure 4. (a) First and (b) second analyzed moving column milling machine.

In Figure 5a, the dynamic characteristics of the third moving column milling machine are shown. Consistent with previous machines, the direct vertical compliance (Φ_{yy}) exhibits the most significant variations. The cross-FRFs (Φ_{xy} , Φ_{yx} and Φ_{yz}) show a reduction in their main resonance amplitude due to the modification of Φ_{yy} compliance. Figure 5b presents a detailed analysis conducted at various axis velocities. The small velocity command, such as 25 mm/min on each axis, leads to modifications in both the amplitude and frequency of the initial idle compliance. Subsequently, increasing the feed command results in varying compliance, reaching a limit where the variation becomes minimal (250 to 500 mm/min) or remains consistent (500 to 1000 mm/min).

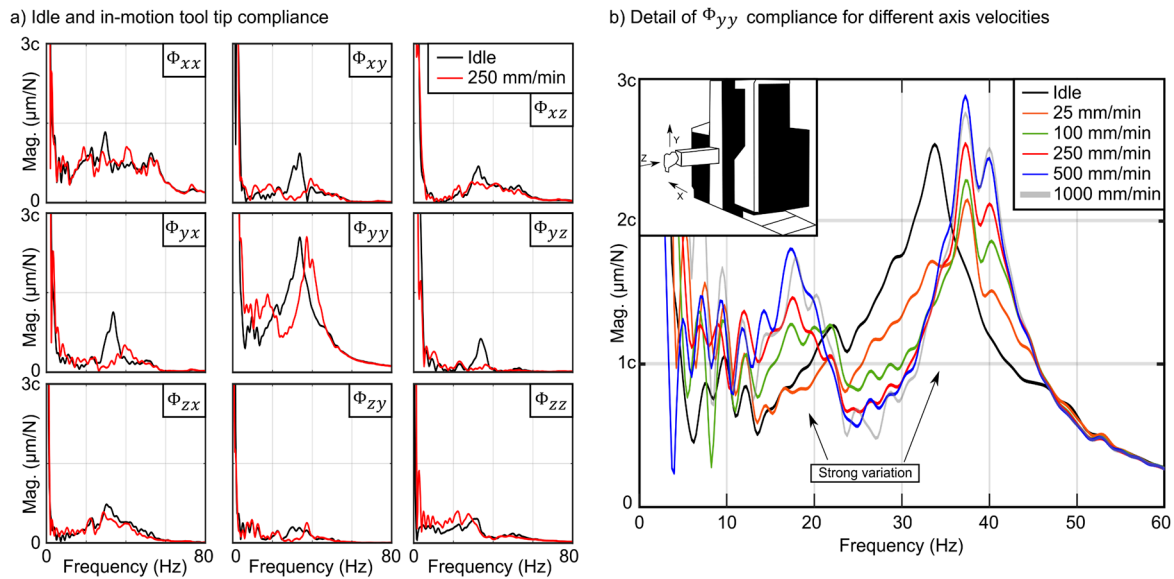


Figure 5. Third analyzed moving column milling machine. (a) Overall view; (b) detail of the Φ_{yy} compliance.

2.4. Portal Milling Machine

Two distinct gantry-type portal milling machines have been analyzed (Figure 1d). In these machines, the x -axis is driven by a gantry master–slave configuration, with each machine leg equipped with a double pinion and rack feed drive system. Meanwhile, the y -axis is powered by a double pinion and rack, while the vertical z -axis utilizes a ball screw drive.

The dynamics of the first studied machine tool are summarized in Figure 6. As a result of the commanded motion trajectory, the main resonance amplitude in Φ_{xx} decreases drastically. In addition, the secondary resonance becomes more pronounced as both its magnitude and frequency characteristics undergo alteration. Similar effects are observed in the Φ_{yy} compliance, where the main resonance differs substantially between idle and in-motion conditions, exhibiting variations in both frequency and damping.

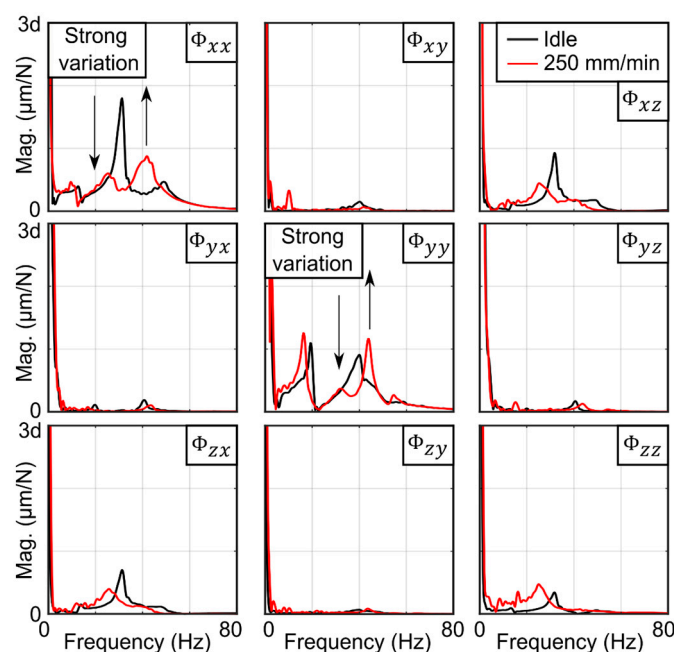


Figure 6. Overall tool center point dynamics for the first portal milling machine.

In the second portal milling machine, the x -axis operates independently from the other two axes through the use of a moving table (the structure of the machine is fixed to the ground). Consequently, the motion of the ram is limited to the vertical and traverse directions (y and z). Figure 7a illustrates the nine FRFs of the ram tip, revealing a decrease in the frequency of the main resonance, accompanied by a significant reduction of 60% in Φ_{xx} , even if there is no feed in the x -direction. In Figure 7b, the evolution of the dynamic compliance for various velocities is depicted, illustrating how the initial idle characteristics converge to a distinct invariant FRF during motion even in the absence of direct x -axis motion.

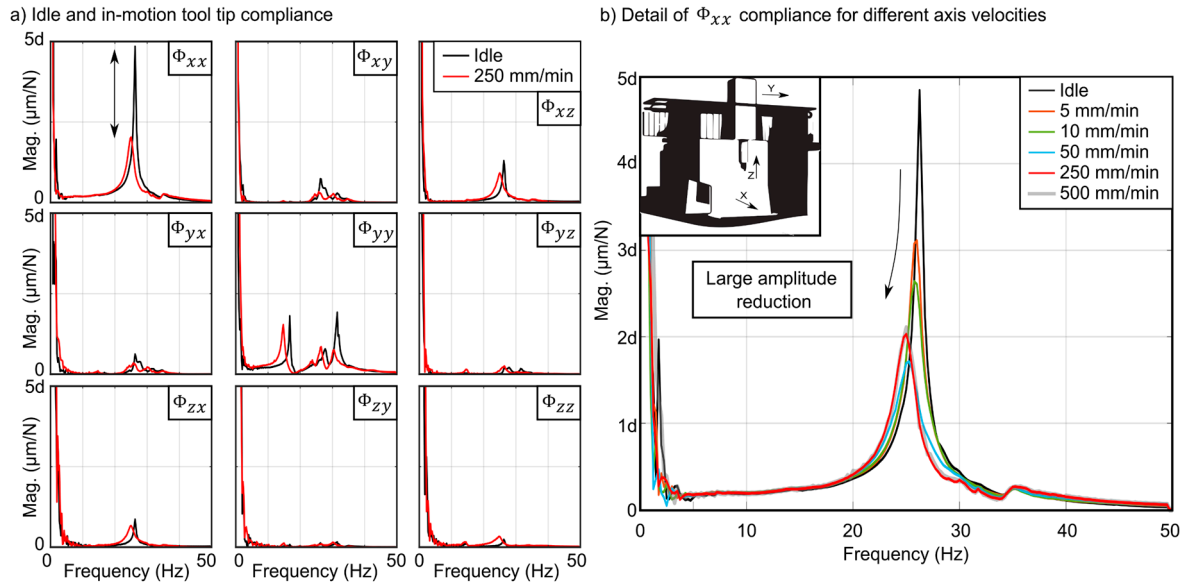


Figure 7. (a) Overall and (b) detail of the machine tool dynamics for the second portal milling machine.

The experimental findings, observed in several industrial machines, provide compelling evidence of the significant influence of axis motion on the tool tip or cutting point dynamics. This influence extends to alterations in both the natural frequency and damping of the main machine tool modes. Recognizing this phenomenon holds crucial implication for various aspects, including the development of model-based active damping techniques, process planning utilizing stability lobes and correlation with finite element models. The next section introduces the different dynamic characterization techniques utilized in this paper.

3. Dynamic Response and Disturbance Force Excitation

The addition of friction introduces non-linearity into the dynamic system. While the concept of Frequency Response Function (FRF) is strictly applicable to linear systems, non-linear systems, like those influenced by friction, are often characterized using the term quasi-FRF, as elucidated by Farago et al. [29]. In this work, the different quasi-FRFs are obtained by different approaches.

3.1. Traditional Impact Hammer

In traditional impact hammer testing, a motion-sensing device (i.e., an accelerometer) measures the vibratory response of the flexible system (\ddot{x}_{tip}), while a dynamometric impact hammer is employed to generate the excitation force (F_{tip}). Both the excitation and response time-domain signals are synchronously acquired, and each frequency-domain response spectrum is computed through Fast Fourier Transform (FFT) analysis. Equation (1) outlines the computation of the quasi-FRF by dividing the cross-spectrum by the input's auto-

spectrum (Ewins [30]). This approach is commonly favored for its efficiency and ease of setup, making it a standard reference against other alternative excitation techniques.

On the other hand, for simulations, the impact hammer force is characterized as a Dirac delta function. This approach enables the study of the machining system’s non-linear sensitivity to various force excitation levels (F_{tip}) or different feedrate commands (\dot{x}_{ref}).

$$\Phi_{quasi}(\omega) = \frac{S_{x_{tip}, F_{tip}}(\omega)}{S_{F_{tip}, F_{tip}}(\omega)} \tag{1}$$

3.2. Inertial Actuator

When addressing non-linear dynamics, it is recognized that the type of excitation can notably impact the computed FRFs (Ewins [30]). Alongside the excitation type, maintaining control over the excitation level is crucial for obtaining reliable results. While electromagnetic shakers are typically preferred for measuring non-linear structure responses, the analyses in this study involve machine movements at varying feeds, a scenario not conducive to traditional hanging shakers. Hence, an inertial actuator employing a linear motor and attached to the moving structure was used. This setup utilizes a Bosch ML3P03-B_BW linear motor to produce a controlled force through the accelerations of an inertial mass. The actuator has been designed in such a way that the primary part of the motor is fixed to the stationary housing, while the coils serve as the inertial moving mass along the motion direction (Figure 8a).

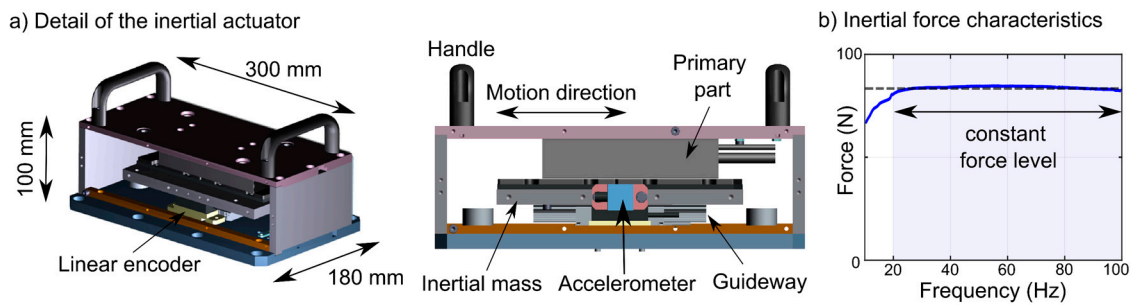


Figure 8. Design and force characteristics of the inertial actuator.

The actuator force characteristics were obtained in the laboratory by using a force dynamometer while entering current commands into the linear drive’s current control loop. Computing the frequency response function between the commanded voltage and the measured force, the actuator’s force characteristics were obtained with a relatively constant force level between 10 Hz and 80 Hz (Figure 8b). With this, the linear motor can generate a controlled force to measure the non-linear dynamics at different force and feed levels.

Once the inertial actuator is placed in the machine’s ram, the excitation involves a constant force stepped-sine ranging from initial to end frequencies over a duration of a certain number of seconds. Two sine waves are matched to the input force and output acceleration to derive the FRF at each frequency point. The magnitude and phase are determined through the ratio of sine wave amplitudes and their phase shift. Additionally, a coherence indicator is computed using the R-squared goodness-of-fit measure.

3.3. Sweep Milling Force Excitation

Alternative identification techniques, such as the Sweep Milling Force Excitation (SMFE) method (Iglesias et al. [4]), offer viable options. Unlike previous methods, like the impact hammer and inertial actuator, SMFE utilizes actual simultaneous cutting forces in the x -, y - and z -directions, variably adjusting the spindle speed. By conducting down, up and central milling operations, independent tests are generated, facilitating a well-conditioned numerical problem for solving the linear system and obtaining the nine machine tool com-

pliances. Further details on the methodology of this alternative characterization technique are extensively discussed in Franco et al. [31].

The next section shows the experimental identification and validation of the friction and controller forces' interaction while characterizing the chatter stability lobes in a single degree-of-freedom system.

4. One-Degree-of-Freedom Modeling

Figure 9 presents the schematic model incorporating friction forces ($F_{friction}$), classical control loops that generate the controller force ($F_{control}$) based on the linear encoder position and velocity feedback measurements (x_{mot} and \dot{x}_{mot}). Additionally, a disturbance force (F_{tip}) can be applied on the flexible structure, as well as motion command to the feed drive system (x_{ref}), allowing the analysis of various feed commands, resulting in different forces generated by the controller and friction and their impact on the tool tip or cutting point dynamic compliance (x_{tip}/F_{tip}). The subsequent section elaborates on the proposed model for each component.

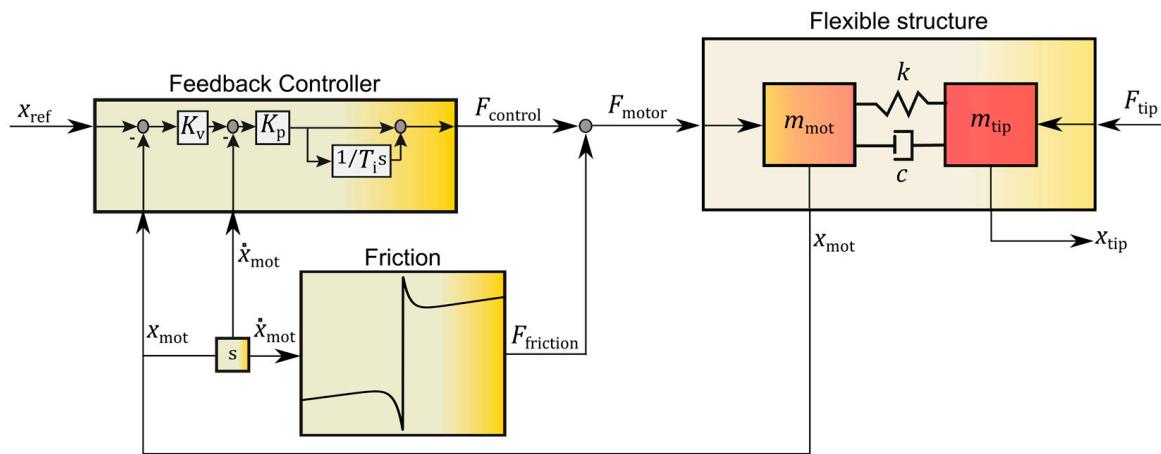


Figure 9. Single-axis feed drive model conceptual description.

4.1. Structural Dynamics

A simplified flexible feed drive system can be dynamically characterized as a two-degree-of-freedom system. The driven load or vibrating structure is represented by m_{tip} and the carriage by m_{mot} (Figure 10). Equation (2) shows the analytical expression of the open-loop system response $(X_{mot}/F_{mot})^{ol}$ with stiffness and damping of the mechanical flexure characterized by k and c , respectively. τ_{ol} represents the delay corresponding to a phase drop due to the sampling rate and the linear motor response. The expression also considers the viscous friction term σ , which modifies the response in the low-frequency range. However, for this research, the effect of viscous friction is not used in this expression, as it is modeled in the friction characteristics described in Section 4.3.

$$\frac{X_{mot}^{ol}}{F_{mot}} = \frac{(m_{tip}s^2 + cs + k)e^{-\tau_{ol}s}}{m_{mot}m_{tip}s^4 + (c(m_{mot} + m_{tip}) + \sigma m_{tip})s^3 + (k(m_{mot} + m_{tip}) + \sigma c)s^2 + \sigma ks} \quad (2)$$

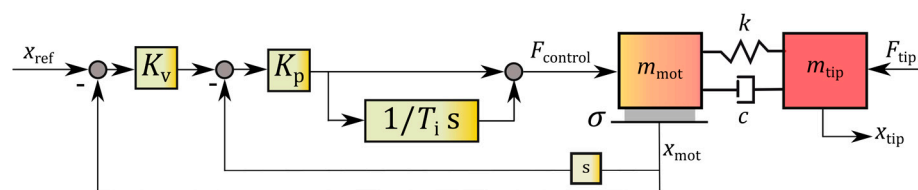


Figure 10. Two-degree-of-freedom model with control loops.

4.2. Feed Drive Control System

Industrial machine tools commonly employ a cascaded loop control structure comprising current, velocity and position feedback loops alongside feedforward action. This structure is often referred to as P–PI cascade control, as the position loop involves a proportional gain, K_v , and the velocity loop is closed with a proportional gain and an integral action (K_p and T_i , respectively). This control scheme offers good parametrization and extensibility with good dynamic characteristics (Gross et al. [32]). The current loop, situated at the innermost level, is closely linked to the motor model. As the tuning of the current loop PI gains is not affected by the machine mechanical modes, the parameters given by the motor manufacturer are often satisfactory. Thanks to the high bandwidth and the sampling time of the loop, it can be modeled as a simple gain K_a (Beudaert et al. [18]). The controller force, F_{control} , depends on the feedback sensor reading, x_{mot} , as shown in Equation (3). It is worth noting that this expression applies specifically to systems utilizing linear motors as feed drive systems, as it does not account for the dynamics associated between rotary and linear encoders present in ball screw or rack and pinion feed drives.

$$F_{\text{control}} = (s + K_v)K_p \left(1 + \frac{1}{T_i s}\right) (X_{\text{ref}} - X_{\text{mot}}) \quad (3)$$

Based on the schematic shown in Figure 10, the following Equation (4) can be obtained to predict the tool center point compliance under the effect of different control parameters, where the viscous friction term (σ) is incorporated. With this, different closed velocity loop bandwidths (f_{bw}) can be proposed to analyze their effect on the cutting point compliance with simplified dynamics. As in the previous case, the consideration of the viscous friction effect of this expression is omitted, as it is incorporated in the proposed friction model of Section 4.3.

$$\frac{X_{\text{tip}}^{\text{cl}}}{F_{\text{tip}}} = \frac{(s + K_v)K_p \left(1 + \frac{1}{T_i s}\right) + m_{\text{mot}}s^2 + cs + k}{(m_{\text{tip}}s^2 + cs + k)(s + K_v)K_p \left(1 + \frac{1}{T_i s}\right) + m_{\text{mot}}m_{\text{tip}}s^4 + (m_{\text{mot}}c + m_{\text{tip}}(\sigma + c))s^3 + ((m_{\text{mot}} + m_{\text{tip}})k + \sigma c)s^2 + \sigma ks} \quad (4)$$

4.3. Friction Characteristics

Friction emerges from the intricate interaction between two surfaces in motion. In 1994, Armstrong et al. [22] described this phenomenon and detailed various models and compensation techniques. Friction behavior typically comprises pre-sliding (or sticking) and sliding regimes, with sophisticated models, like Generalized Maxwell-Slip (GMS, Al-Bender et al. [33]), capturing the characteristics before full slip. However, their complexity poses challenges for identification and dynamic simulations (Hagman [34], Andersson et al. [35]). To address discontinuities at low speeds, continuous velocity-based functions are employed, assuming zero friction force at zero velocity. In this research, the Andersson tanh-type model in Equation (5) is utilized for its smooth transition to full sliding and suitability for transient oscillation simulation (Andersson et al. [35]). However, this velocity-dependent model sacrifices accuracy in final position prediction compared to dynamic friction models. Parameters F_c and F_s represent Coulomb and static friction, while σ denotes the viscous friction coefficient. Additionally, k_t regulates the rate of friction force change near pre-sliding and sliding stages, with v_s representing the sliding speed coefficient and δ the velocity shape factor.

$$F_{\text{friction}} = \left[F_c + (F_s - F_c)e^{-\left(\frac{|\dot{x}_{\text{mot}}|}{v_s}\right)^\delta} \right] \tanh(k_t \dot{x}_{\text{mot}}) + \sigma \dot{x}_{\text{mot}} \quad (5)$$

5. Laboratory Test Bench Experimental Validation

Figure 11 illustrates the setup used to construct the previously described model in Section 4. It features a single axis driven by an ETEL ILM06-06-3RB-A20C linear motor (ETEL S.A., Môtiers, Switzerland), with an added flexure supporting the workpiece on

top of the slider. The flexure is designed to have a natural frequency of 60 Hz in the motion direction, enhancing the observability and controllability via the feed drive control system. As for the control system, the ETEL controller closes the current loop, while an external dSPACE DS1005PPC controller (dSPACE GmbH, Paderborn, Germany) manages the position, velocity and command trajectory. Note that the test bench was initially located in a granite base to conduct the fundamental characterizations and model validation. Then, the single-axis drive was positioned within a HAAS CNC machine tool (Haas Automation, Inc., Oxnard, CA, USA), allowing for milling cutting tests.

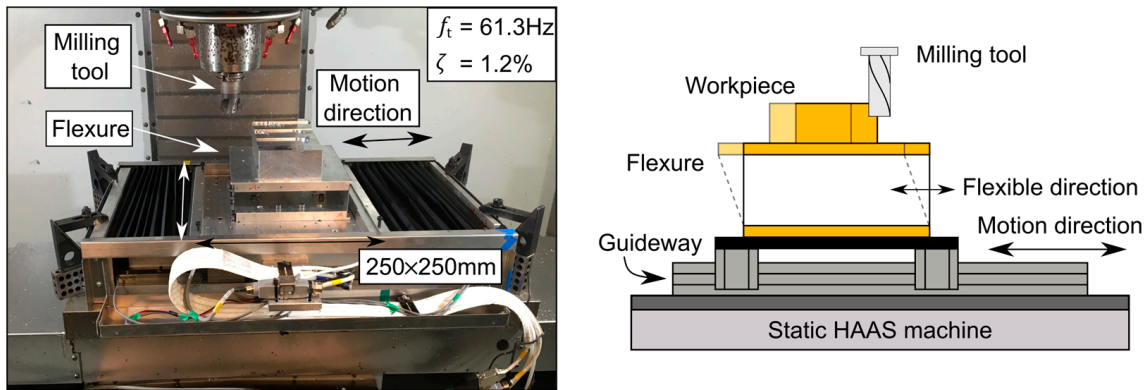


Figure 11. Laboratory experimental setup within the HAAS milling machine.

5.1. Identification of Model Parameters

The model parameters representing the structural dynamics were extracted from an experimental open-loop response measurement $(X_{mot}/F_{mot})^{ol}$ using Equation (2) (as illustrated in black color in Figure 12). A pseudo-random binary sequence input was applied to the experimental setup while the axis was moving at 500 mm/min. As a result, the setup stayed on the sliding friction regime; hence, only the viscous friction component affected this measurement. Additionally, the excitation force was selected to avoid generating motion reversals. The natural frequency of the flexure $f_t = 61.3$ Hz, known as the motor-locked frequency, corresponds to the anti-resonance of the motor’s open-loop response, where load-side vibrations cancel out the displacement of the motor mass. Due to the combination of inertias and stiffness, resonance is generated at $f_r = 75$ Hz. As previously noted, the effect of the viscous friction term in the low-frequency range is evident, particularly in the phase response (gray vs. red fitted response). This viscous friction term effect (σ) will be incorporated within the externally coupled friction model. Additionally, the phase drop at higher frequencies, primarily due to the sampling rate, is also accounted for in the model. The extracted model parameters are summarized in Table 1 and represent the gray color response.

Table 1. Summary of the identified dynamic and friction parameters.

Dynamic parameters				
m_{mot}	m_{tip}	k	c	τ_{ol}
23.1 kg	11.3 kg	1.68 N/ μm	104 Ns/m	0.75 ms
Andersson model friction parameters		Positive direction	Negative direction	
Coulomb sliding friction (F_c)		44.2 N	38.7 N	
Maximal static friction (F_s)		84 N	88 N	
Sliding speed coefficient (v_s)		387.4 mm/min	421 mm/min	
Viscous friction coefficient (σ)		0.0028 Nmin/mm	0.0025 Nmin/mm	

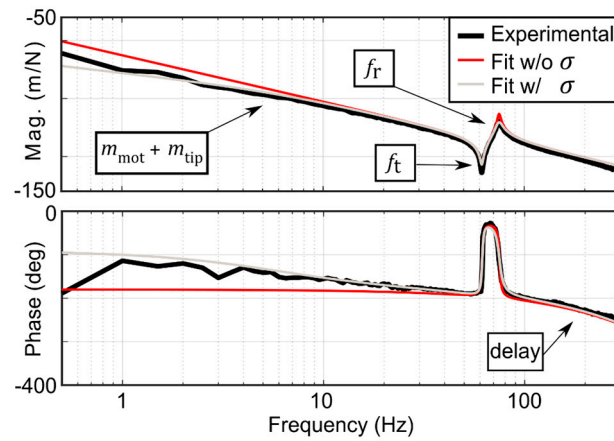


Figure 12. Experimental and fitted open-loop response function.

The friction force characteristics are identified by running the test bench at different steady-state sliding feeds and computing the average motor force while the axis is commissioned with a very low-control bandwidth, effectively isolating the friction effects. Figure 13a shows the experimental and computed mean values of motor force for continuous displacements performed at 25 and 1500 mm/min. Figure 13b shows the fitted friction model over the experimentally characterized points. The extracted model parameters, which have been obtained by the minimization of the RMS error, are summarized in Table 1; note that the model constant (k_t) is 0.25 min/mm and the velocity shape factor (δ) is 1 for both positive and negative directions.

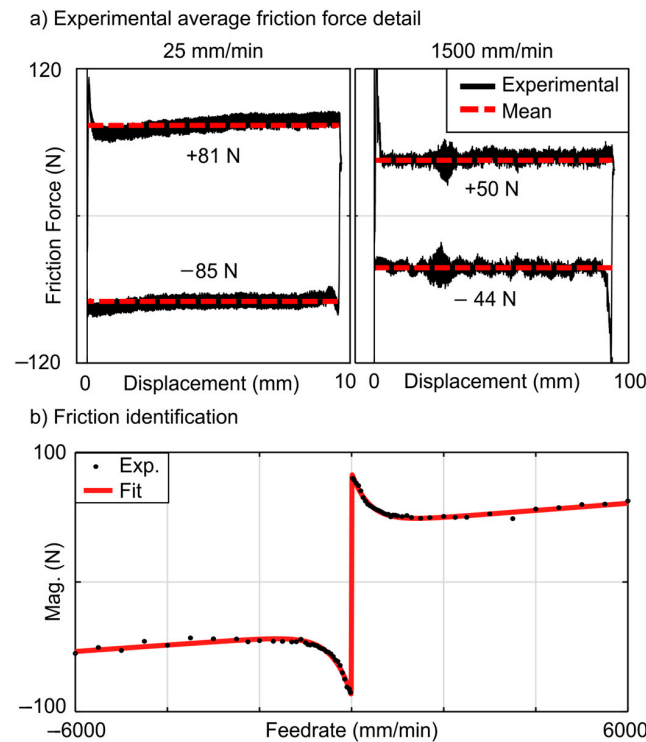


Figure 13. (a) Experimental friction identification; (b) friction model fitting.

5.2. Analysis of the Control and Friction Force Interactions

The experimental and simulated quasi-FRFs were obtained using the traditional impact hammer testing approach. For the simulations, the excitation amplitude was chosen based on the experimental impact tests conducted on the test bench flexure, using a PCB 086C03 hammer with a soft rubber tip. The cutting point displacement (x_{tip}) was simulated

in response to the externally applied force at the same point (F_{tip}) while considering the influence of the servo feedback control ($F_{control}$) and guideway friction ($F_{friction}$). Figure 14a shows the cutting point quasi-FRF simulation and experimental compliances for different axis feeds with a 25 N excitation force. For the idle machine case ($\dot{x}_{ref} = 0$ mm/min), the dynamic compliance exhibits a poorly damped resonance coming from the flexure at 61.3 Hz. As the commanded feed increases, the in-motion FRF varies significantly, both in amplitude and frequency, up to a certain feedrate level ($\dot{x}_{ref} = 500$ mm/min), where the dynamic response becomes ‘invariant’. This change results from the interaction between the servo controller and friction forces for different feedrate commands (Figure 14b). This can be further explained by the following:

- For the idle case ($\dot{x}_{ref} = 0$ mm/min), the reference feedrate is zero, resulting in the servo controller force being negligible compared to the friction force ($F_{friction} \gg F_{control}$), resulting in the idle or static dynamic response.
- As the reference feedrate increases, the servo controller force also increases, leading to interactions between the control and the friction forces ($F_{friction} \approx F_{control}$).
- Above a certain feedrate ($\dot{x}_{ref} \approx 500$ mm/min), the servo controller force becomes dominant, resulting in a linear system response (i.e., less amplitude-dependent) and the dynamic compliance remains ‘invariant’ ($F_{friction} \ll F_{control}$). This allows the effect of the selected servo bandwidth (f_{bw} , i.e., $f_{bw1} = 0.8f_t$ and $f_{bw2} = 0.4f_t$) on the obtained dynamic response to be observed.

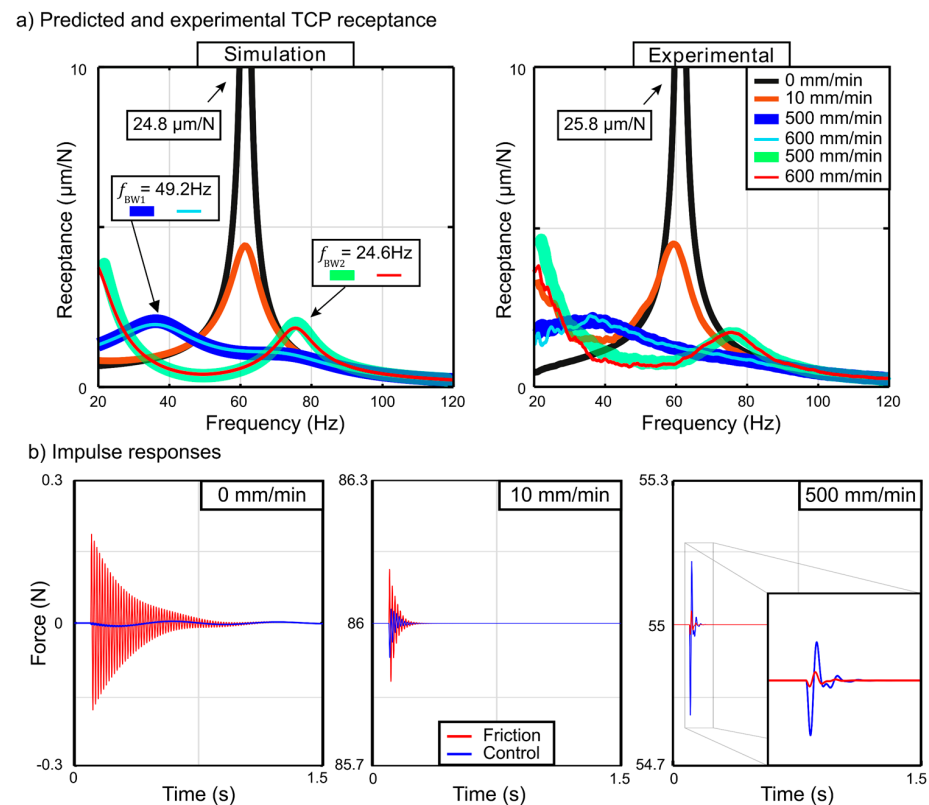


Figure 14. (a) Simulated and experimental idle and in-motion FRFs; (b) simulation variation of different force sources for different axis feeds.

The proposed model represents the experimental trend with high fidelity under different feed levels and controller bandwidths. Therefore, using this model, various friction models are proposed to analyze the idle and in-motion FRF prediction capabilities. Three different friction models are considered (Figure 15a): the previously described Andersson-type friction model in Equation (5); a model that considers only the viscous friction component (σ); and a third configuration that neglects the Stribeck effect by considering both

Coulomb and viscous friction effects. This third model can be derived from Equation (5) by equalizing the maximal static (F_s) and Coulomb (F_c) sliding friction values. Figure 15 summarizes the cutting point dynamics with these different friction models. Figure 15c shows the compliance results using the viscous friction component alone, which fails to capture the effect of machine idle conditions. This is because the controller-generated force, even in idle conditions, is much more dominant than the friction-generated force. Similar results are obtained when friction characteristics are omitted from the simulation. By using the combined viscous and Coulomb model, the machine’s idle, in-motion and ‘invariant’ dynamics can be predicted. However, some amplitude deviations exist compared to those obtained with the Andersson friction model, which has been previously validated experimentally.

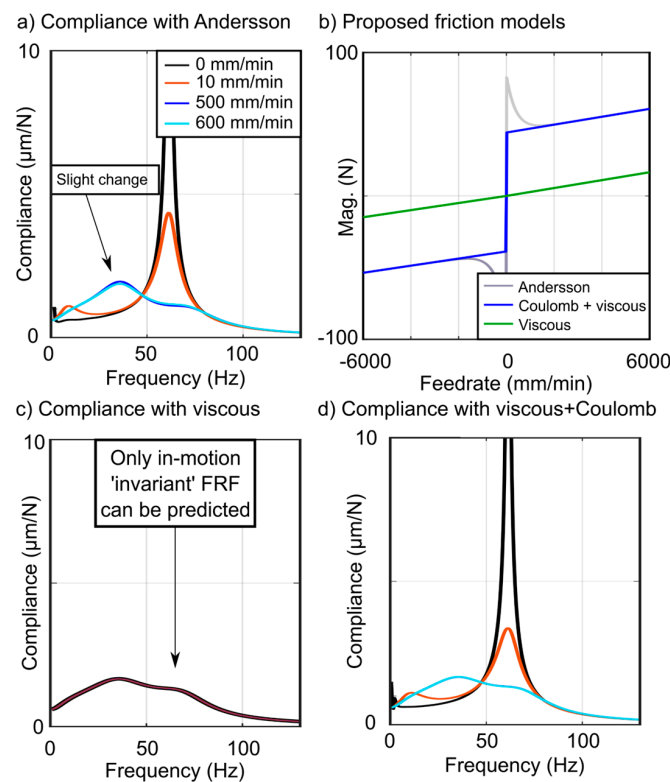


Figure 15. Friction models and equivalent quasi-FRF simulations.

Utilizing the Andersson-type friction model enables accurate simulation of the transition between idle and in-motion ‘invariant’ quasi-FRF, consistent with experimental findings. Conversely, while the Coulomb with viscous friction model offers a good approximation with minimal modeling effort, it may provide less precise predictions of compliance during the transition between idle and motion invariant states.

After the fundamental behavior was described, the single-axis feed drive test bench was relocated from granite to a HAAS CNC machine tool, which allows for milling stability tests. For that, the first step was to characterize the cutting point compliance, as illustrated in Figure 16. As a result of the relocation, the idle cutting point dynamics were affected by the flexibility of the host milling machine (a small resonance at 45 Hz and an antiresonance at 48 Hz), disturbing the ideal behavior of a single degree of freedom but representing conditions close to industrial applications.

As the in-motion dynamics are affected by the commissioned control bandwidth, Table 2 summarizes the four different proposed control parameter sets. Figure 16 shows the impact of varying the closed velocity loop bandwidth on the cutting point dynamics. By employing the parameters extracted in Section 5.1 and applying Equation (4), different control parameter sets can be proposed to predict the cutting point dynamics during motion

and follow the expected trend from advanced analysis tools, such as root locus [18]. The experimental FRFs were obtained by an impact hammer while the setup was moving at a constant feedrate of 500 mm/min. For this case, it can be seen how the control loops modify the dynamic compliance between two asymptotic cases. The first case refers to the open-loop response with zero static stiffness ($K_p = 0$), the second case corresponds to $K_p \rightarrow \infty$, where m_{mot} is completely fixed due to the high controller stiffness, and the two degrees of freedom model behaves like a single suspended mass with the main resonance frequency at 61 Hz.

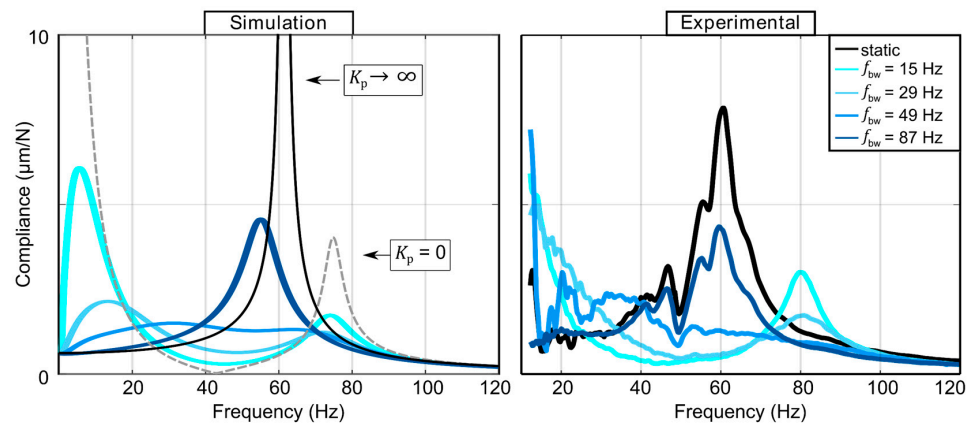


Figure 16. Simulated and experimental in-motion FRFs for various control parameters.

Table 2. Commissioned control parameters for the laboratory setup.

	f_{bw} (Hz)	K_p (Ns/m)	T_i (ms)	K_v (1/s)
K1	15	3242	21.2	23.5
K2	29	6268	10.9	45.5
K3	49	10,590	6.5	76.9
K4	87	18,804	3.6	136.6

5.3. Influence of Excitation Force Level on the Quasi-FRF

Using the simulation model of Section 4, Figure 17 shows cutting point quasi-FRFs for different excitation levels (25 N and 1000 N) at both idle and a 500 mm/min feedrate. The modification of the feedrate is the primary factor causing significant variations in dynamics between idle and in-motion states, whereas changes in the excitation level result in only minor variations in the dynamic response.

The dynamic variations attributed to friction have a direct impact on the prediction of stability lobes, explaining the potentially large deviations between the predicted and experimentally measured stability limits. The following section discusses experimental milling tests conducted to validate the variation in system dynamics during cutting operations.

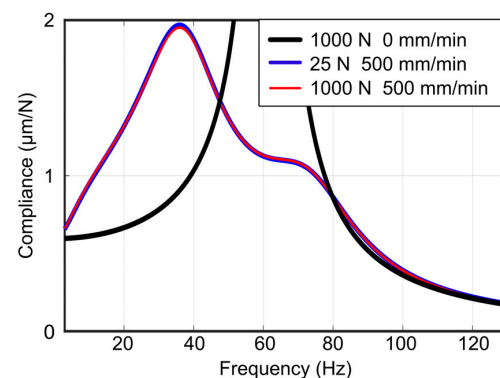


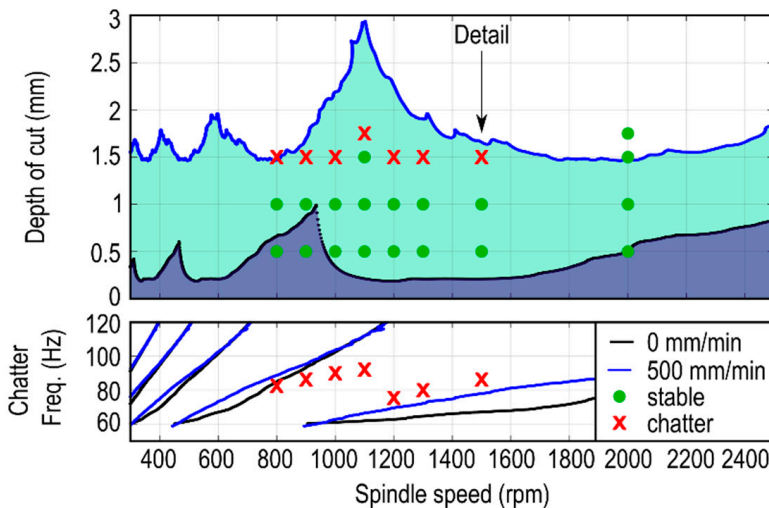
Figure 17. Influence of the excitation force on the simulated compliance.

5.4. Process Stability Analysis

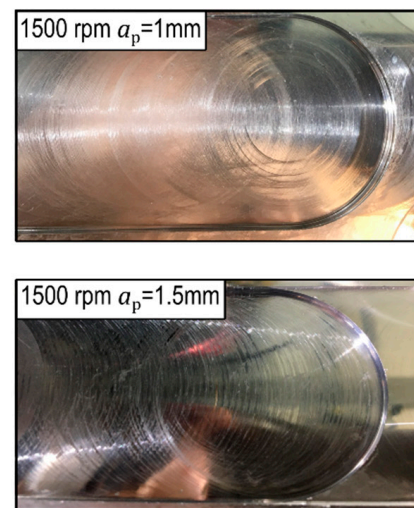
By using the frequency responses indicated in Figure 16, the milling chatter stability lobes are computed following the approach of Altintas et al. [36] for idle and in-motion invariant dynamics (under the effect of maximum damping controller K2), considering a secant-type linearization around the operating condition. As previously indicated, the test bench was placed in a HAAS VF2YT machine table, and the feed was provided by the single-axis test bench. The stability lobes were predicted for a full immersion cutting operation using a 50.8 mm diameter tool with four straight inserts. Dedicated cutting tests were performed to characterize the aluminum 6061 material, obtaining $K_{tc} = 780 \text{ N/mm}^2$ and $K_{rc} = 351 \text{ N/mm}^2$ cutting coefficients. The vertical direction was very stiff, and a tool with an approach angle of 90 degrees was used, so a 2D stability model was applied. A feed per tooth of 0.2 mm/Z ensures that even for the lowest spindle speed of 800 rpm, the axis velocity is higher than the in-motion ‘invariant’ feed of 500 mm/min.

Figure 18a shows the experimental stability lobes on top of the theoretical predictions, where in-motion characterization predicts the cutting capabilities much better than the classical static one. The following criteria to identify the presence of chatter is based on the peaks of the vibration spectrum. Chatter is detected if a non-harmonic vibration peak amplitude is higher than half of the amplitude of the highest tooth-passing frequency harmonic (Figure 18c).

a) Experimental verification of chatter stability predictions



b) Experimental surface finish



c) Vibration spectra detail for 1500 rpm

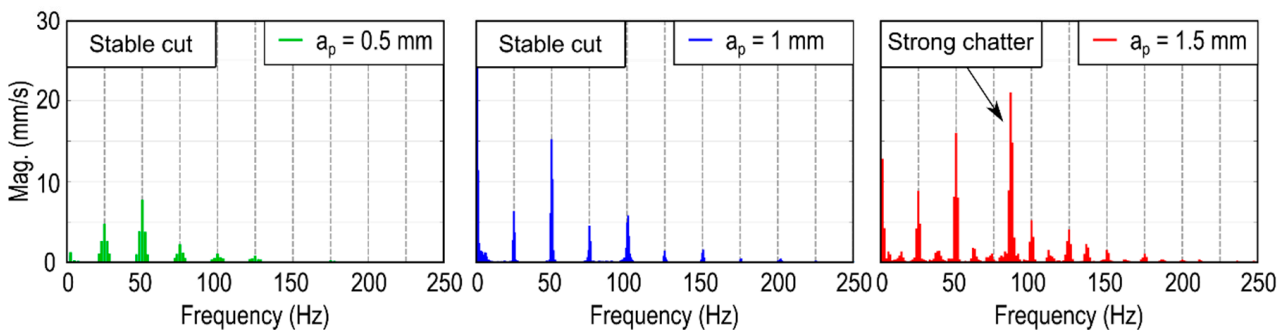


Figure 18. Summary of the experimental process stability results.

It can be concluded that more accurate predictions of the process stability are obtained using the in-motion acquired quasi-FRF over the idle one when dealing with simplified dynamics. Bearing this in mind, the next section analyzes a large-scale machine tool with more complex dynamics.

6. Large-Scale Machine Tool Validation

Figure 19a shows a ram-type multitasking machine tool with milling, turning and grinding capabilities used for the industrial validation of the impact of guideway friction characteristics on chatter stability prediction accuracy. A double pinion and rack feed drive system was used in the x horizontal direction, as the traveling stroke is above 4 m, whereas a ball screw drive was employed in the y - and z -directions. The machine was controlled by a Heidenhain TNC640 CNC, which utilizes the classical P–PI cascaded controller; note that an electronic preload was imposed by a master–slave coupling for the double pinion and rack feed drive mechanism.

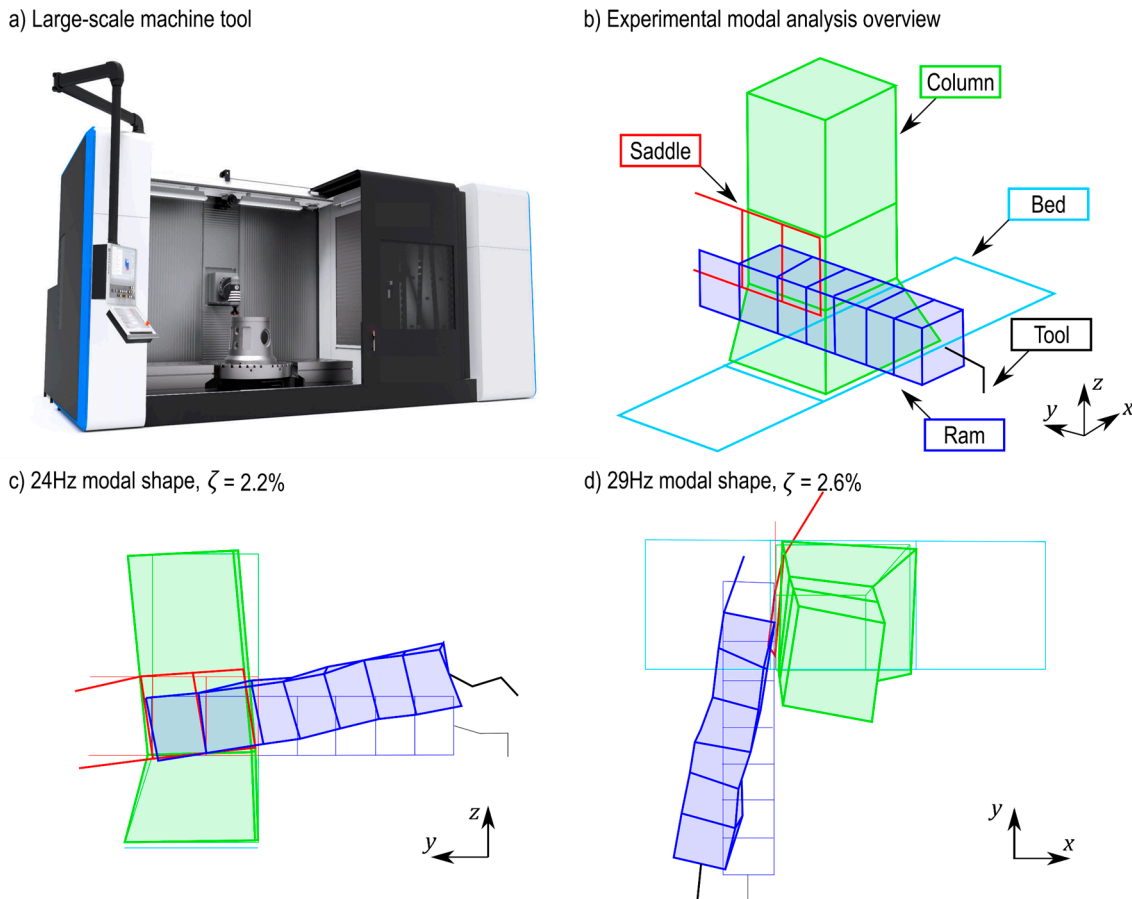


Figure 19. (a) Large-scale machine tool overview; (b) overview of the experimental modal analysis. (c) Modal shape of the 24 Hz frequency; (d) modal shape of the 29 Hz frequency.

A modal analysis of the machine tool was carried out to characterize the machine tool dynamic behavior (Figure 19b). The machine was excited in the two flexible directions (x and y) using a dynamometric impact hammer. Among the different natural frequencies, the modal shapes of the critical resonances that limit the machine’s cutting capabilities are described. Notably, prior process stability tests were conducted to identify these resonances. First, the mode shape at 24 Hz consisted of a rotation of the saddle and ram in phase with the bending of the column in the yz plane (Figure 19c) with a damping of 2.2%. Then, at 29 Hz there was another rotation of the saddle and ram in phase with the torsion of the column in the xy plane (Figure 19d) with a damping of 2.6%. These shapes show the existing rotations and displacements between the different main machine tool components, where the axis guideways and feedback sensors are located.

6.1. Feed Influence on Tool Center Point Dynamics

The measured variations in tool tip compliances due to different axis feeds are summarized in Figure 20 (for confidentiality, the exact values of magnitude are not disclosed in the frequency response measurements. Instead, alternative values labeled ‘a’ are used to protect sensitive data). These frequency response functions were obtained using impact hammer tests, with all three axes moving at the specified feed. The modification of the machine’s posture, which is less than 30 mm, has minimal influence on the observed dynamic variations. Collocated measurements were performed by exciting and measuring at the tool tip. To ensure accurate characterization, a device with flat faces, rather than a conventional insert tool, was employed to facilitate proper excitation.

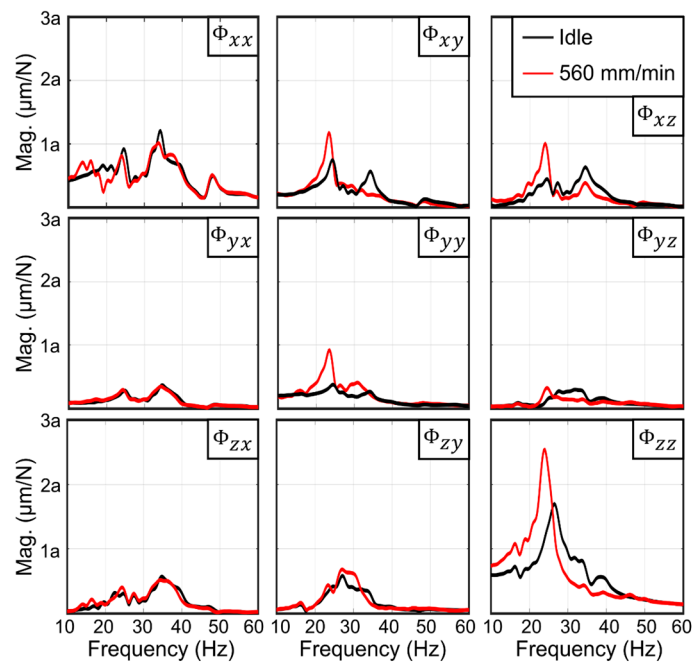


Figure 20. Tool tip compliance at idle and motion conditions measured with an impact hammer in a large-scale machine tool.

When analyzing the measured results when excited in the x -direction, it was determined that the overall dynamic behavior of the machine remained relatively stable without any drastic changes. However, in the direct response Φ_{xx} , a noticeable dynamic amplification phenomenon occurred around 15 Hz. Changing to the ram overhang axis, the direct Φ_{yy} frequency response function shows that the primary vibration mode exhibited a notable shift, characterized by a decrease in its natural frequency of 6.1%. Additionally, this frequency reduction was accompanied by a significant increase in the amplitude of 58%. A similar trend was observed in the cross Φ_{xy} response, where the frequency decreased a 6.1% and the magnitude increased a 36.8%. Finally, addressing the vertical direction, the direct Φ_{zz} response reveals a marked change in the system’s behavior. The initial shape observed under idle conditions was modified, resulting in an undamped response, increasing its magnitude by 28%.

Based on the obtained responses, the following subsection focuses on the feed drive control parametrization for each individual axis. By adjusting these parameters, the aim is to modify the dynamic response of the machine tool, ultimately enhancing its cutting capabilities.

6.2. Feed Drive Servo Control Loop Tuning

Considering the effect the control parametrization can have in the tool tip dynamics, two different feed drive control sets are proposed for the validation presented in this section.

The first set, referred to as K1, is a reference controller tuned with a primary focus on the CNC Bode plots. The goal is to maximize the tracking performance of the machine axis, which leads to the use of high controller gains. While commissioning the CNC, in addition to ensuring a mandatory stable control loop, the following guidelines can be adhered to:

- The closed velocity loop amplitude Bode plot must be limited to +3 dB. During the machining process, the disturbances should be tackled as fast as possible; therefore, an overshoot of up to 3 dB is generally accepted in the velocity loop.
- The closed position loop amplitude Bode plot must be limited to 0 dB, meaning that no overshoot is allowed, as it will be reflected in the geometrical characteristics of the machined workpiece.

On the other hand, a secondary control parameter set is proposed that maximizes the achievable damping of the mechanical system. As previously observed in Section 5, to fully observe the control actuation force, it is essential that the machine axis operates within the viscous friction regime. For this purpose, a representative feed velocity of 560 mm/min was selected during the commissioning stage. This feedrate is common for heavy-duty applications (spindle speed $n = 350$ rpm, feed per tooth $f_z = 0.2$ mm/tooth and number of tool teeth $Z = 8$) and places the feed drive within the viscous linear region of the friction curve (see Section 4.3). By commanding a back-and-forth trajectory at this specific traverse speed, different controllers are defined to achieve optimal performance.

Figure 21 presents the direct frequency response function of the x -axis at the machine ram while traveling at 560 mm/min, with the dynamic behavior at idle conditions included for comparison. As previously mentioned, the principal resonance dynamic behavior does not change significantly with different controllers, likely due to the modal shape’s minimal projection on the x -axis control system. However, the low-frequency region shows abrupt changes. The expected resonance at 18 Hz shifts to different frequencies depending on the selected bandwidth. By decreasing the velocity loop proportional gain while maintaining a reasonably low integral time (i.e., 10 ms), it can be seen how the control pole generated by the integral action of the velocity loop emerges. Therefore, lowering the K_p gain requires an increment on the integral time parameter (T_i) to avoid this resonance. The high coherence indicator across all the control parameterizations suggests reliable measurements.

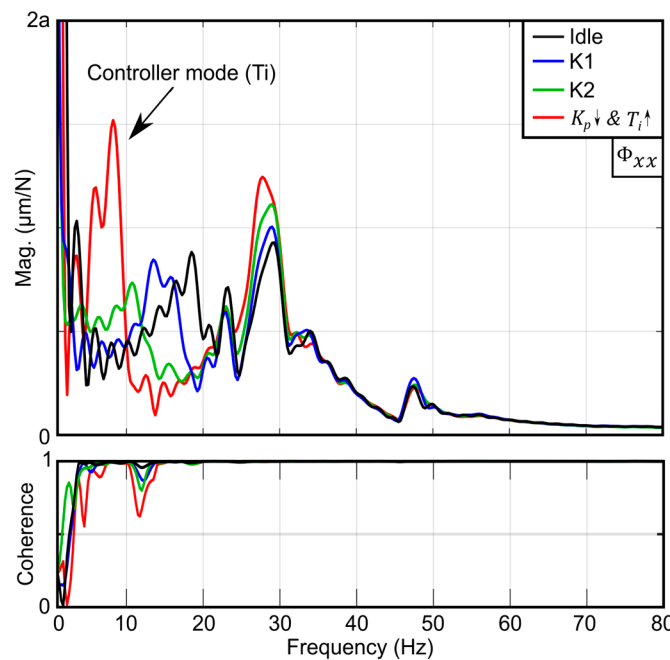


Figure 21. Axis dynamic compliance with different control sets while in motion.

Figure 22 illustrates the impact of different control parameters on the remaining two axes. In the case of the y-axis, corresponding to the ram overhang direction, a notable variation in compliance was observed between the idle and in-motion conditions for the primary flexible resonance at 24 Hz. It is apparent that the high bandwidth K1 controller induced a more flexible response compared to the lower bandwidth alternative. Moreover, an inadequately tuned $K_p - T_i$ parametrization can lead to a significant resonance in the low-frequency range, despite achieving improved magnitude at frequencies relevant to the chatter stability. It is worth noting that the low-frequency range can be excited during machine movements while cutting, necessitating a favorable trade-off between these aspects. However, strategically coupling the controller pole with the mechanical pole, as demonstrated by the K2 controller, can yield an overall enhanced response. Similarly, the response of the z-axis (vertical) mirrors the observed trends in the y-axis behavior. Note that for the three axes, the controller impact on the experimental cutting point compliance can only be seen when the feed is higher than 0 mm/min. These measurements experimentally demonstrate the substantial impact of the feed magnitudes on defining machine tool compliance, thus potentially altering the expected stability outcomes significantly.

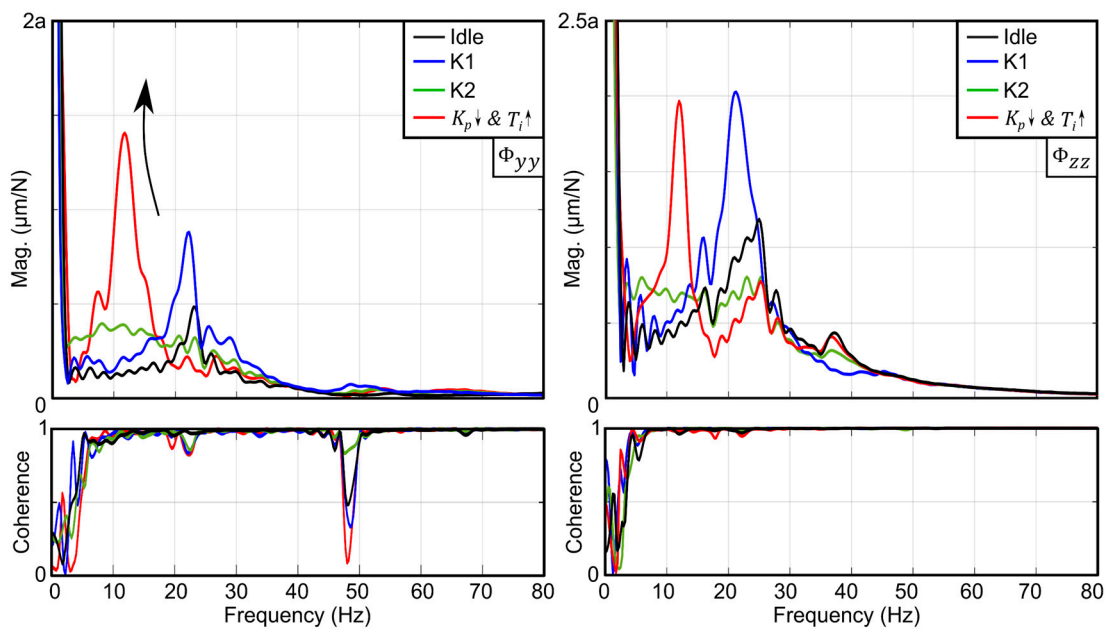


Figure 22. y- and z-axis dynamic compliance with different control sets while in motion.

6.3. Single-Axis Feed and Force Non-Linearities

As it has been previously simulated for the laboratory test bench, it is proposed now to study the effect of excitation force and feed amplitude on large-scale machine tool compliances. While electromagnetic shakers are typically preferred for their precise force control, allowing analysis of non-linearities like force amplitude dependency or friction, hanging shakers are unsuitable for detecting in-motion frequency response functions. Hence, the use of a linear motor drive was proposed to be used as an inertial actuator (see Section 3.2).

Given the posture-dependent dynamics of the machine, the actuator was positioned in the machine ram to act along the x-direction, where the dynamics of the feed drive mechanism are independent of the traveling distance (Figure 23a). Note that this direction will be used as the cutting direction for future process stability tests. The excitation was carried out using a constant force stepped sine of 50, 100 and 150 N, ranging from 10 to 60 Hz over 86 s. Figure 23 illustrates that under idle conditions, compliances at 24 Hz and 34 Hz decrease as the force level rises, indicating a force-related non-linearity. The resonance at 33 Hz is notably influenced by the excitation force, with an 8.4% and 20%

decrease in magnitude observed at 100N and 150N, respectively. Conversely, the natural frequency at 24 Hz shows minor variation with increasing force (8% and 16%). However, unlike the 33 Hz resonance, this frequency demonstrates high sensitivity to feed. The dynamic behavior between 10 Hz and 30 Hz undergoes abrupt changes with increasing feed, which is consistent with the findings from the impact hammer tests.

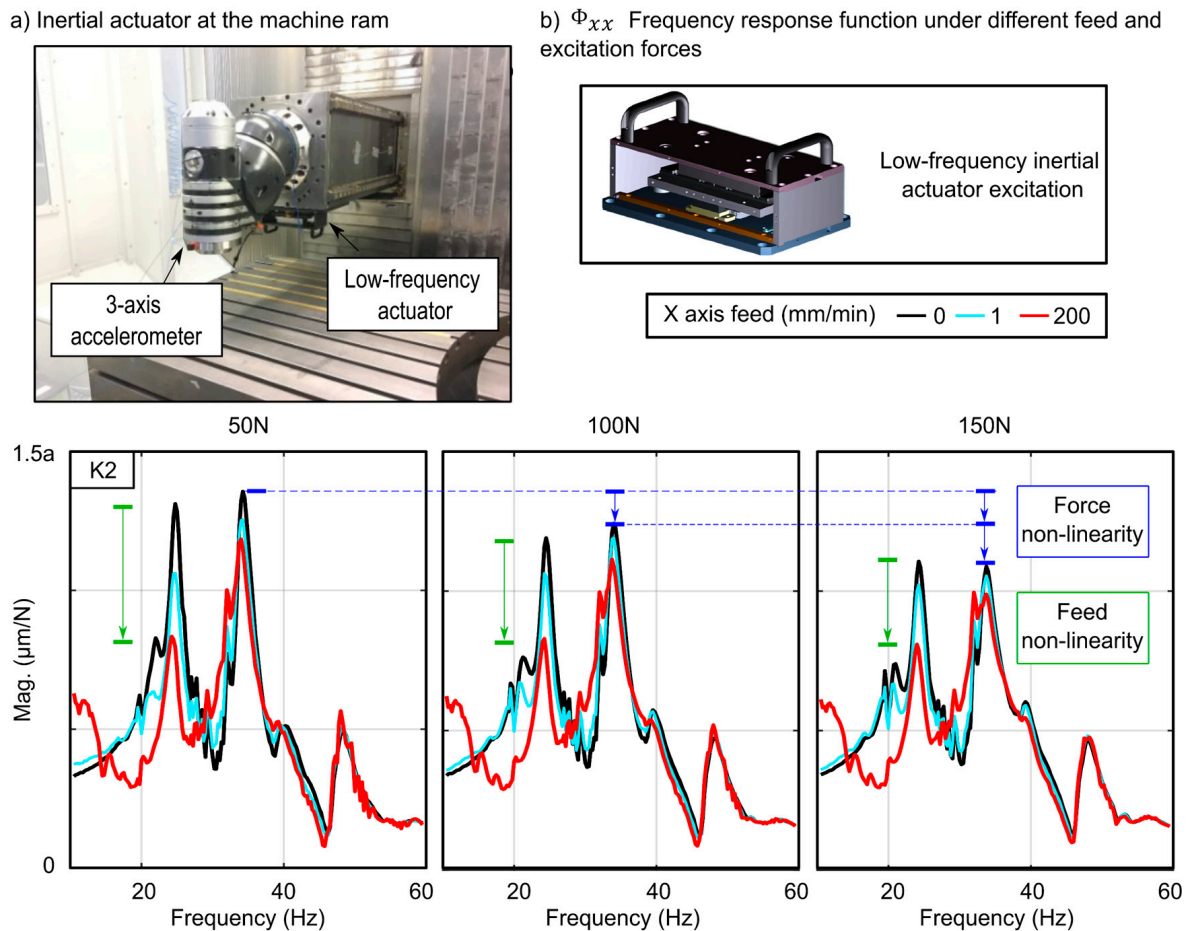


Figure 23. Machine tool dynamic response through inertial actuator excitation for different excitation forces and feeds.

These measurements experimentally demonstrate the substantial impact of both excitation force and feed magnitudes on defining machine tool compliance, thus potentially altering the expected stability outcomes significantly. While the conducted analysis of this subsection has been focused on a single axis with varying controlled forces and feeds, it is essential to recognize that during the cutting process, the machine undergoes multi-axial excitation (depending on the tool’s or insert’s geometry). Consequently, the following subsection analyzes the process stability prediction accuracy for different conditions (idle vs. moving) and identification techniques (hammer vs. alternative SMFE).

6.4. Process Stability Prediction and Experimental Validation

The stability lobes theory assumes linear dynamics to predict chatter stability. In this analysis, the classical zero-order stability model is applied, considering the measured frequency responses as linearization around the operating condition. A 125 mm diameter tool with 8 inserts and a 45-degree approach angle was used to perform a down-milling operation in C45 steel. The feed per tooth was set to 0.2 mm/z in the positive *x*-direction.

The variations in tool tip compliances due to different axis feeds introduce uncertainties in the dynamics used to estimate the stability limits. Figure 24 illustrates the measured

changes in tool tip compliances as a function of axis feeds. These frequency response functions were obtained through impact hammer tests conducted with all the axes moving at the specified feedrates. Notably, alterations in the machine posture, within a range of less than 30 mm, have minimal impact on the observed dynamic variations. As discussed in previous sections, the parameterization of the drive control system can significantly alter the dynamic response at high speeds. This modification affects not only the direct responses but also the cross terms.

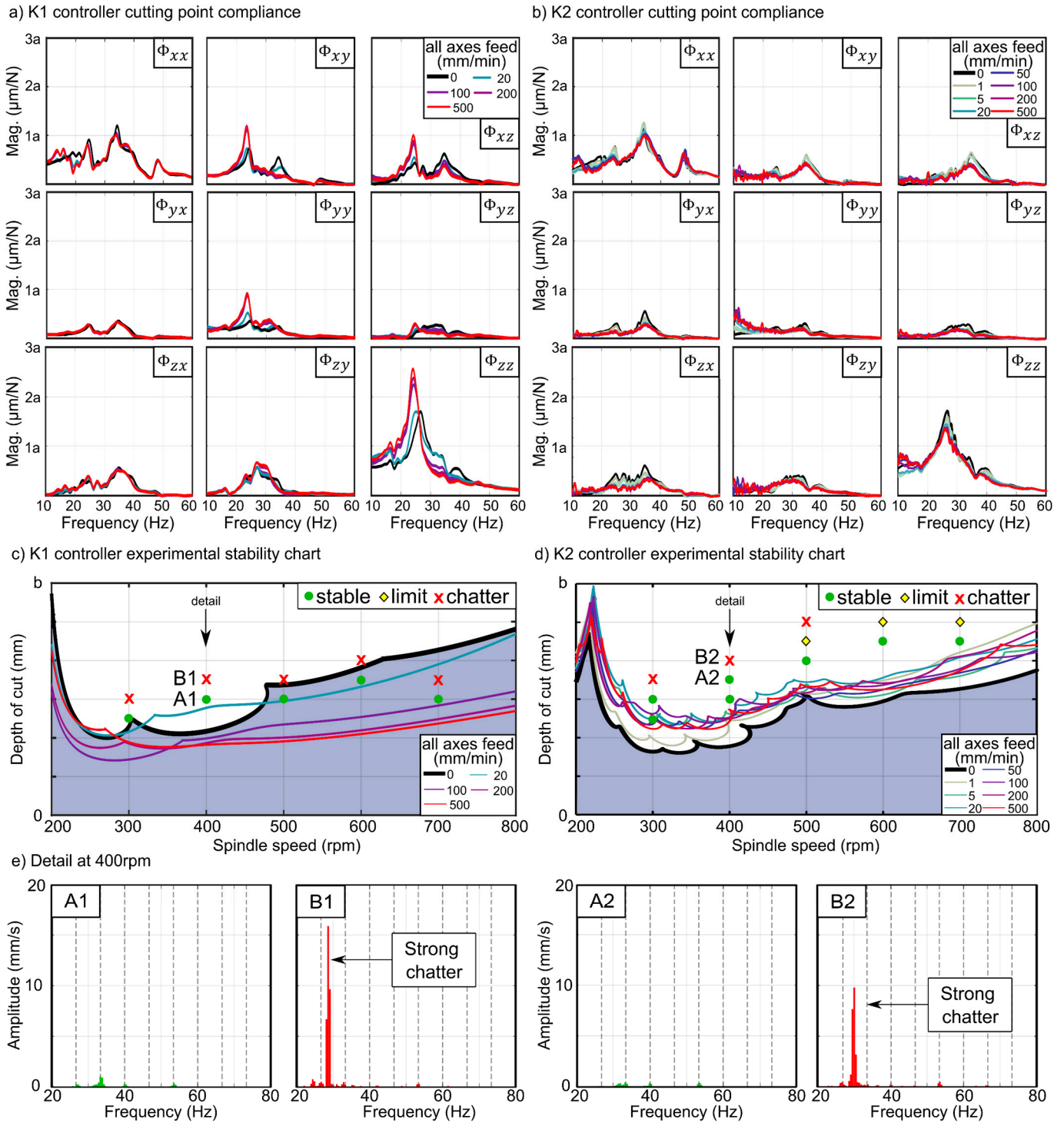


Figure 24. Experimental characterization through impact hammer tests and process stability.

Analyzing the experimental results of process stability, a correct parametrization of the feed drive system can increase the cutting capabilities of the driven machine significantly (minimum improvement of 16% at 400 rpm and maximum of 50% at 700 rpm). Even greater differences could be expected in this machine if other directions were used as the primary cutting direction, given the significant dynamic variations observed from idle to in-motion states and between the K1 and K2 controllers (see Section 6.2). However, the current implementation of SMFE is limited by posture-dependent dynamics. Despite these limitations, the findings demonstrate an overall enhancement in machine cutting capabilities and a generalized reduction in vibration amplitude. This reduction in vibrations not only improves the cutting performance but also extends the life of machine components. Additionally, the bandwidth reduction will enlarge the geometric precision, so this approach is particularly interesting for initial roughing operations. On the contrary, more aggressive tuning parameters of controller K1 can be used for subsequent finishing operations, optimizing the overall machining process.

Focusing now on the process stability predictions, for the case of the K1 controller, the hammer tests in static conditions provided accurate estimates at speeds of 300, 500 and 600 rpm. However, major errors occurred at 400 and 700 rpm. The stability predictions based on measurements with the axes in motion indicated a lower cutting capability than the machine can deliver. This discrepancy may be due to two main factors. First, as noted in Section 6.3, the magnitude of certain resonances decreases with increasing excitation force levels, an effect not considered in these measurements. Second, during characterization, all three axes were in motion simultaneously, whereas in the actual cutting process, the x -axis delivers the primary cutting direction. For the case of the K2 controller, an improvement in predicting the stability limit was observed when using the in-motion characterizations. Nonetheless, a margin of error persisted, likely due to non-linear effects related to the level of excitation force. To account for these deviations, the machine was characterized using the SMFE technique (Section 3.3).

Figure 25 illustrates the dynamic responses obtained through this alternative characterization method, employing different levels of excitation forces and both controllers. Analyzing the direct response along the x -axis (Φ_{xx}) for the K2 controller, it becomes clear that the magnitude of the main peak at 34 Hz was significantly influenced by the excitation force. Higher excitation forces led to a reduction in peak amplitude, with decreases of 16% and 27% observed at 1.5 mm and 2 mm depths of cut, respectively. Additionally, dynamic variations in the low-frequency range were also present under this excitation. These observations are consistent with the findings from the previous sections, which utilized a low-frequency inertial actuator and traditional impact hammer tests. Turning to the direct response along the z -axis, it can be noted that the response differed from that obtained using the classical impact hammer approach. However, the compliance in this direction did not exhibit significant variations with changes in the excitation level. This consistency indicates that while the excitation force affected the x -axis response markedly, its impact on the z -axis response was less pronounced. Note that only a pass with a 2 mm depth of cut was conducted for the machine under the effect of the K1 controller.

Comparing the process stability limit prediction based on the different characterization techniques, a significant difference was observed across the analyzed spindle speed range. Focusing on the results of the K1 controller, the predictions obtained through impact hammer testing tended to be more conservative. However, comparing to the experimental stability results, it can be concluded that more accurate predictions can be obtained through the SMFE technique. A similar pattern was replicated in the stability predictions under the effect of the K2 controller, where the SMFE technique can accurately predict the process stability boundary. Additionally, slight variations in the frequency response functions can lead to substantial differences in the stability lobes. Considering that the experimental chatter frequency for this cutting operation fell between 30 and 37 Hz, the experimental results from the hammer and sweep milling tests were similar in this range, except for the Φ_{zz} and Φ_{yz} compliances, which showed significant variations depending

on the excitation method. Therefore, the multi-axis feed and force variations of operational excitations alter the expected direct- and cross-FRFs, impacting the stability predictions. This behavior was similarly observed when using the high-gain K1 controller, indicating that the control parameter selection and characterization methodology significantly influence stability predictions. These findings underscore the importance of accurate dynamic characterization to improve the reliability of stability lobe predictions and, consequently, the overall cutting performance.

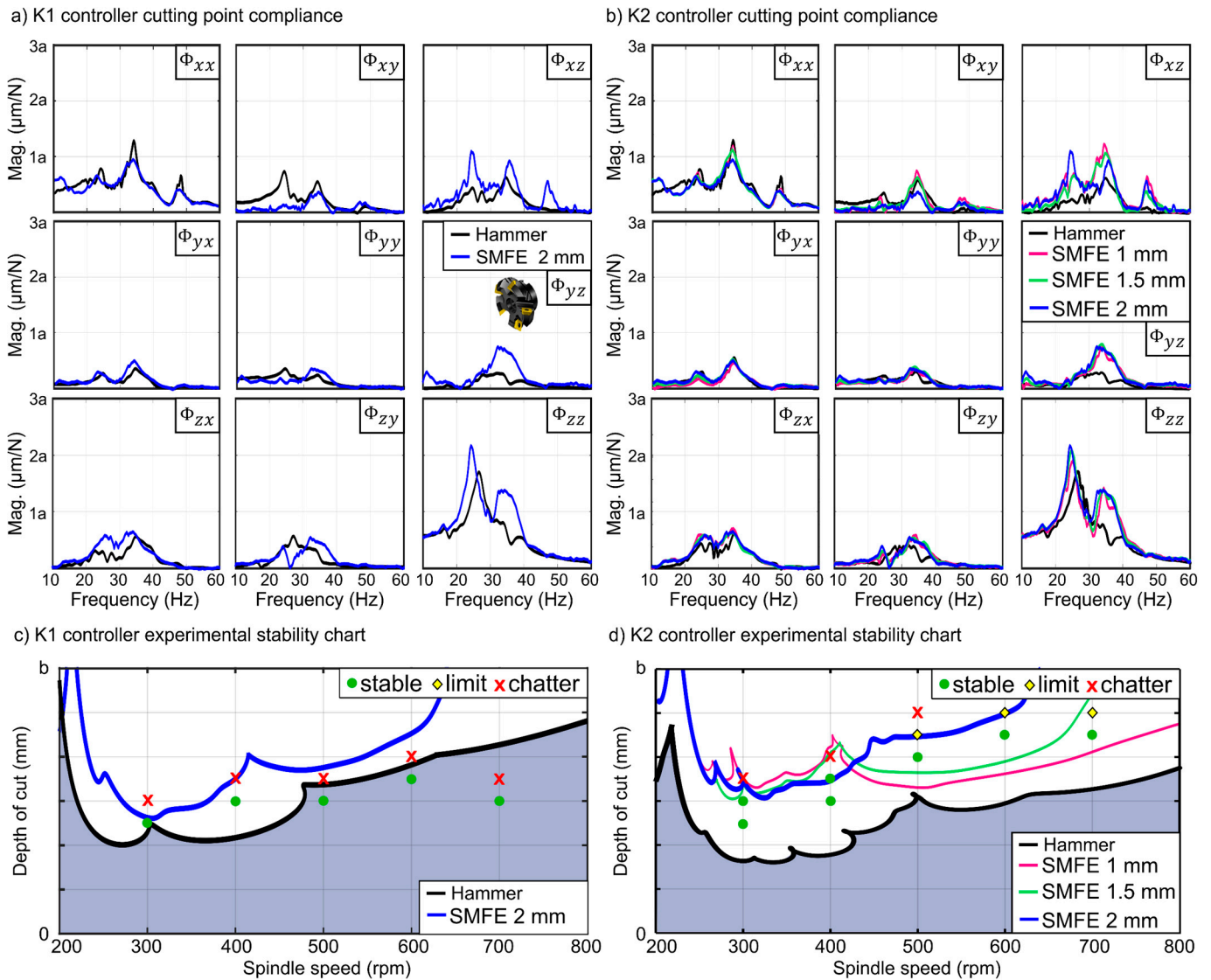


Figure 25. SMFE characterization and process stability predictions.

7. Conclusions

Variations in tool tip compliance with axis feeds in large-scale machine tools introduce uncertainties in predicting chatter stability limits. These coupled with the effects of servo control during motion reduce the accuracy of stability predictions. While dynamometric hammers are widely used for quick dynamic characterization, non-linearities, such as mechanical clearances and friction, limit their effectiveness. The lack of control over excitation force and frequency further complicates rigorous analysis, although they do allow measurements at the cutting point and provide insights into feed drive control effects.

To address these limitations, electromagnetic actuators are proposed for their precise force control. Traditional methods using hanging shakers are constrained by travel range, limiting the study of non-linearities associated with machine feeds. This paper introduces a

solution by mounting the actuator near the cutting point, enabling analysis of force-related non-linearities across different frequencies. Although feed-based stability predictions improve, accuracy is compromised when the excitation is not localized at the cutting point. The alternative SMFE technique, which tests various force levels by adjusting the depth of cut, offers a more reliable approach for dynamically complex machines, despite limitations due to posture-dependent dynamics.

The most relevant conclusions are as follows:

- Experimental dynamic characterization of different large-scale machine tools and a robot with milling capabilities revealed significant variations in compliance between idle and in-motion conditions, impacting both the amplitude and frequency of resonances.
- A one-degree-of-freedom model incorporating friction and control forces, along with motion commands, is presented.
- Simulations with different friction models indicated that considering both Coulomb and viscous friction is sufficient to accurately estimate in-motion invariant receptance.
- Laboratory test bench experiments showed that relying solely on idle frequency response functions (FRFs) can lead to significant prediction deviations.
- It was found that a low proportional velocity loop gain combined with aggressive integral action minimizes damping of the pole generated by the integral action, appearing in the measured FRF at the cutting point. This effect was prominent in ball screw and double pinion and rack feed drives during motion.
- An inertial actuator was used to analyze the effects of the axis feed and force on machine tool dynamics, concluding that both non-linearities can be present and affect different frequency ranges individually.
- The observed force and feed non-linearity on the frequency response function at the cutting point directly affects the shape of the predicted stability lobes, especially for the K2 controller.
- Two different feed drive control parameter sets were implemented on an industrial machine tool. This study provides guidelines for correctly characterizing machine tool dynamics under in-motion conditions. Up to 50% productivity improvement can be achieved by correctly selecting control gains.

Following the line of the work discussed in this research, the following steps can be targeted:

- Development of an alternative SMFE technique that can handle posture-dependent dynamics;
- Finite element modeling of complex machine dynamics considering friction and control influences;
- Analysis and investigation of optimal control laws that remain optimal even in the presence of dynamic modifications due to feed non-linearities;
- Investigation of the modification of the guideway frictional response to improve the machine cutting capabilities;
- Incorporation of different non-linear effects to enhance the accuracy of process stability predictions.

Author Contributions: Conceptualization, X.B., K.E. and J.M.; investigation, O.F. and X.B.; writing, O.F.; supervision, X.B., K.E. and J.M. All authors have read and agreed to the published version of the manuscript.

Funding: This research was funded by the Basque Country Business Development Agency (SPRI) ELKARTEK 2024 MECACOGNIT (KK-2024/00030) research and collaborative project.

Data Availability Statement: Data are contained within the article.

Conflicts of Interest: The authors declare no conflicts of interest.

References

1. Munoa, J.; Beudaert, X.; Dombovari, Z.; Altintas, Y.; Budak, E.; Brecher, C.; Stepan, G. Chatter suppression techniques in metal cutting. *CIRP Ann.* **2016**, *65*, 785–808. [[CrossRef](#)]
2. Brecher, C.; Esser, M. Stability prediction: Advances and current restrictions. In Proceedings of the 6th International Conference on High-Speed Machining, San Sebastian, Spain, 21–22 March 2007.
3. Rasper, P.; Rott, O.; Hömberg, D.; Uhlmann, E. Analysis of uncertainties in the stability prediction for milling processes. In Proceedings of the CIRP 2nd International Conference Process Machine Interactions, Trondheim, Norway, 10–11 June 2010.
4. Iglesias, A.; Tunc, L.T.; Özşahin, O.; Franco, O.; Munoa, J.; Budak, E. Alternative experimental methods for machine tool dynamics identification: A review. *Mech. Syst. Signal Process.* **2022**, *170*, 108837. [[CrossRef](#)]
5. Xu, H.; Hinze, C.; Lechler, A.; Verl, A. Robust μ parameterization with low tuning complexity of cascaded control for feed drives. *Control Eng. Pract.* **2023**, *138*, 105607. [[CrossRef](#)]
6. Sun, Z.; Pritschow, G.; Zahn, P.; Lechler, A. A novel cascade control principle for feed drives of machine tools. *CIRP Ann.* **2018**, *67*, 389–392. [[CrossRef](#)]
7. Neubauer, M.; Brenner, F.; Hinze, C.; Verl, A. Cascaded sliding mode position control (SMC-PI) for an improved dynamic behavior of elastic feed drives. *Int. J. Mach. Tools Manuf.* **2021**, *169*, 103796. [[CrossRef](#)]
8. Zhang, L.; Liu, J.; Zhuang, C.; Yao, M.; Chen, F.; Zhang, C. Gain scheduling control of ball screw feed drives based on linear parameter varying model. *Int. J. Adv. Manuf. Technol.* **2023**, *124*, 4493–4510. [[CrossRef](#)]
9. Dumanli, A.; Sencer, B. Active control of high frequency chatter with machine tool feed drives in turning. *CIRP Ann.* **2021**, *70*, 309–312. [[CrossRef](#)]
10. Dumanli, A.; Sencer, B. Active chatter mitigation by optimal control of regenerative machining process dynamics. *IEEE/ASME Trans. Mechatron.* **2021**, *27*, 3165–3173. [[CrossRef](#)]
11. Kakinuma, Y.; Enomoto, K.; Hirano, T.; Ohnishi, K. Active chatter suppression in turning by band-limited force control. *CIRP Ann.* **2014**, *63*, 365–368. [[CrossRef](#)]
12. Uriarte, L.; Zatarain, M.; Axinte, D.; Yagüe-Fabra, J.; Ihlenfeldt, S.; Eguia, J.; Olarra, A. Machine tools for large parts. *CIRP Ann.* **2013**, *62*, 731–750. [[CrossRef](#)]
13. Altintas, Y.; Verl, A.; Brecher, C.; Uriarte, L.; Pritschow, G. Machine tool feed drives. *CIRP Ann.* **2011**, *60*, 779–796. [[CrossRef](#)]
14. Zirn, O. Machine Tool Analysis-Modelling, Simulation and Control of Machine Tool Manipulators. Habilitation Thesis, ETH, Zürich, Switzerland, 2008.
15. Franco, O.; Beudaert, X.; Erkorkmaz, K. Effect of rack and pinion feed drive control parameters on machine tool dynamics. *J. Manuf. Mater. Process.* **2020**, *4*, 33. [[CrossRef](#)]
16. Grau, J.; Souček, P.; Sulitka, M. The influence of servo drive control on the NC vertical milling machine dynamic compliance. *J. Manuf. Mater. Process.* **2020**, *4*, 111. [[CrossRef](#)]
17. Albertelli, P.; Cau, N.; Bianchi, G.; Monno, M. The effects of dynamic interaction between machine tool subsystems on cutting process stability. *Int. J. Adv. Manuf. Technol.* **2012**, *58*, 923–932. [[CrossRef](#)]
18. Beudaert, X.; Franco, O.; Erkorkmaz, K.; Zatarain, M. Feed drive control tuning considering machine dynamics and chatter stability. *CIRP Ann.* **2020**, *69*, 345–348. [[CrossRef](#)]
19. Li, C.; Xu, M.; Song, W.; Zhang, H. A review of static and dynamic analysis of ball screw feed drives, recirculating linear guideway, and ball screw. *Int. J. Mach. Tools Manuf.* **2023**, *188*, 104021. [[CrossRef](#)]
20. Koenigsberger, F.; Tlustý, J. *Machine Tool Structures*; Elsevier: Amsterdam, The Netherlands, 2016.
21. Zhang, G.P.; Huang, Y.M.; Shi, W.H.; Fu, W.P. Predicting dynamic behaviours of a whole machine tool structure based on computer-aided engineering. *Int. J. Mach. Tools Manuf.* **2003**, *43*, 699–706. [[CrossRef](#)]
22. Armstrong-Hélouvy, B.; Dupont, P.; De Wit, C.C. A survey of models, analysis tools and compensation methods for the control of machines with friction. *Automatica* **1994**, *30*, 1083–1138. [[CrossRef](#)]
23. Bianchi, G.; Cagna, S.; Cau, N.; Paolucci, F. Analysis of vibration damping in machine tools. *Procedia CIRP* **2014**, *21*, 367–372. [[CrossRef](#)]
24. Zaeh, M.F.; Rebelein, C.; Semm, T. Predictive simulation of damping effects in machine tools. *CIRP Ann.* **2019**, *68*, 393–396. [[CrossRef](#)]
25. Sato, R.; Noguchi, S.; Hokazono, T.; Nishida, I.; Shirase, K. Time domain coupled simulation of machine tool dynamics and cutting forces considering the influences of nonlinear friction characteristics and process damping. *Precis. Eng.* **2020**, *61*, 103–109. [[CrossRef](#)]
26. Oshita, I.; Matsubara, A.; Sumida, T. Evaluation of dynamic characteristics of a hybrid guideway system. *Int. J. Autom. Technol.* **2020**, *14*, 274–279. [[CrossRef](#)]
27. Tunc, L.T.; Gonul, B. Effect of quasi-static motion on the dynamics and stability of robotic milling. *CIRP Ann.* **2020**, *70*, 305–308. [[CrossRef](#)]
28. Franco, O.; Beudaert, X.; Erkorkmaz, K.; Munoa, J. Influence of guideway friction on the cutting point receptance in machine tools. *CIRP Ann.* **2022**, *71*, 361–364. [[CrossRef](#)]
29. Farago, D.; Dombovari, Z. Experimental study on free vibratory behavior of nonlinear structure. *Period. Polytech. Mech. Eng.* **2019**, *63*, 91–99. [[CrossRef](#)]
30. Ewins, D.J. *Modal Testing: Theory, Practice and Application*; John Wiley & Sons: Hoboken, NJ, USA, 2009.

31. Franco, O.; Beudaert, X.; Iglesias, A.; Dombovari, Z.; Erkorkmaz, K.; Munoa, J. Optimal cutting condition selection for high quality receptance measurements by sweep milling force excitation. *Int. J. Mach. Tools Manuf.* **2022**, *176*, 103873. [[CrossRef](#)]
32. Gross, H.; Wiegartner, G.; Hamann, J. *Electrical Feed Drives in Automation: Basics, Computation, Dimensioning*; John Wiley & Sons: Hoboken, NJ, USA, 2001.
33. Al-Bender, F.; Lampaert, V.; Swevers, J. The generalized Maxwell-slip model: A novel model for friction simulation and compensation. *IEEE Trans. Autom. Control* **2005**, *50*, 1883–1887. [[CrossRef](#)]
34. Hagman, L.A. Measurement and Modelling of Microslip for Engineering Surfaces in Contact. Ph.D. Thesis, KTH, Stockholm, Sweden, 1997.
35. Andersson, S.; Söderberg, A.; Björklund, S. Friction models for sliding dry, boundary and mixed lubricated contacts. *Tribol. Int.* **2007**, *40*, 580–587. [[CrossRef](#)]
36. Altıntaş, Y.; Budak, E. Analytical prediction of stability lobes in milling. *CIRP Ann.* **1995**, *44*, 357–362. [[CrossRef](#)]

Disclaimer/Publisher’s Note: The statements, opinions and data contained in all publications are solely those of the individual author(s) and contributor(s) and not of MDPI and/or the editor(s). MDPI and/or the editor(s) disclaim responsibility for any injury to people or property resulting from any ideas, methods, instructions or products referred to in the content.